Optogenetic tools for manipulation of cyclic nucleotides, functionally coupled to CNG-channels

Thilo Henß[1,2] | Jatin Nagpal[1,2,3] | Shiqiang Gao[4] | Ulrike Scheib[5,6] | Alessia Pieragnolo[7] | Alexander Hirschhäuser[1,2,8] | Franziska Schneider-Warme[9] | Peter Hegemann[5] | Georg Nagel[4] | Alexander Gottschalk[1,2]

1 Buchmann Institute for Molecular Life Sciences, Goethe University, Max von Laue Strasse 15, D-60438 Frankfurt, Germany
2 Institute of Biophysical Chemistry, Goethe University, Max von Laue Strasse 9, D-60438 Frankfurt, Germany
3 current address: APC Microbiome Ireland, University College Cork, Cork, Ireland.
4 Department of Neurophysiology, Institute of Physiology, Biocentre, Julius-Maximilians-University, D-97070 Würzburg, Germany
5 Institute for Biology, Experimental Biophysics, Humboldt-Universität zu Berlin, 10115 Berlin, Germany
6 current address: NUVISAN ICB GmbH, Müllerstrasse 178, D-13353 Berlin, Germany
7 University of Padova, Faculty of Pharmacy, Padova, Italy
8 Institute for Physiology and Pathophysiology, Department of Molecular Cell Physiology, Philipps-University Marburg, Marburg, Germany
9 Institute for Experimental Cardiovascular Medicine, University Heart Center, Medical Center – University of Freiburg and Faculty of Medicine, Elsässer Str. 2Q, 79110 Freiburg, Germany

Correspondence

Alexander Gottschalk, Buchmann Institute for Molecular Life Sciences and Institute of Biophysical Chemistry, Goethe-University, Max-von-Laue Str. 15, D-60438 Frankfurt, Germany, Email: a.gottschalk@em.uni-frankfurt.de

Funding information

This work was funded by the Deutsche Forschungsgemeinschaft (DFG), grants SPP1926 and CRC807, P11.

Data availability

The data is available on request from the authors.

Author contribution

Conceived experiments: TH, AG. Performed experiments, analysed data: TH, AP. Provided reagents: JN, SQ, US, AH, FS-W, PH, GN. Wrote the paper: TH, AG. Acquired funding and supervised the project: AG.

Conflict of interest

The authors declare no conflict of interests.

Ethics approval

Not applicable, all experiments were performed using invertebrates or cell lysates.

Abbreviations:

Arch, *Halorubrum sodomense* archaerhodopsin-3; BeCNG1, *Blastocladiella emersonii* cyclic-nucleotide-gated channel; BeCyclOp, *Blastocladiella emersonii* guanylyl cyclase Opsin; bPAC, *Beggiatoa* photoactivatable adenylyl cyclase; BWM, body wall muscle; CaCyclOp, *Catenaria anguillulae* guanylyl cyclase Opsin; ChR2, Channelrhodopsin-2; CNG, cyclic nucleotide-gated; CNGC, cyclic nucleotide-gated channel; cNMP, cyclic nucleotide monophosphate; euPAC, *Euglena* photoactivatable adenylyl cyclase; GtACR, *Guillardia theta* anion channel rhodopsin; mb, membrane-bound; NC, nucleotidyl cyclases; NpHR, *Natronomonas pharaonis* halorhodopsin; PAC, photoactivatable adenylyl cyclase; PGC, photoactivatable guanylyl cyclase; SthK, *Spirochaeta thermophila* cAMP-gated K^+-channel; SV, synaptic vesicle

Bullet point summary

What is already known

- Impairment of cNMP signalling is linked to various diseases e.g. neurodegeneration, cardiovascular disorders

What this study adds

- In-vivo test system for the characterization of photoactivatable nucleotidyl cyclases
- Optogenetic tools for cNMP production, coupled to CNG channels to de- or hyperpolarize cells

What is the clinical significance

- Implementation of photoactivatable nucleotidyl cyclases to facilitate pharmaceutical research

Background and Purpose

The cyclic nucleotides cAMP and cGMP are ubiquitous second messengers participating in the regulation of several biological processes. Interference of cNMP signalling is linked to multiple diseases and thus is an important component of pharmaceutical research. The existing optogenetic toolbox in *C. elegans* is restricted to soluble adenylyl cyclases, the membrane-bound *Blastocladiella* CyclOp and hyperpolarizing rhodopsins, yet missing are membrane-bound photoactivatable adenylyl cyclases and hyperpolarizers on the basis of K^+-currents.

Experimental Approach

For the characterization of the photoactivatable nucleotidyl cyclases, we expressed the proteins alone or in combination with cyclic-nucleotide gated channels in *C. elegans* muscle cells and cholinergic motor neurons. To investigate the extent of optogenetic cNMP production and the ability of the systems to de- or hyperpolarize the cells, we performed behavioural analyses (locomotion, muscle contraction) and measured the cNMP content *in vitro*.

Key Results

We implemented *Catenaria* CyclOp as a new tool for cGMP production, allowing fine-control of cGMP levels. As photoactivatable membrane-bound adenylyl cyclases, we established YFP::BeCyclOp(A-2x) and YFP::CaCyclOp(A-2x), enabling more specific optogenetic cAMP signalling compared to soluble ACs. For the hyperpolarization of excitable cells by K^+-currents, we introduced the cAMP-gated K^+-channel SthK from *Spirochaeta thermophila* with either bPAC or BeCyclOp(A-2x), and the *Blastocladiella emersonii* cGMP-gated K^+-channel BeCNG1 with BeCyclOp.

Conclusion and Implications

We established a comprehensive suite of optogenetic tools for cNMP manipulation for the nematode, which will be useful for applications in many cell types, including sensory neurons which use mainly cGMP as second messenger, and for potent hyperpolarization using K^+-ions.

Keywords

Cyclic nucleotide gated channels, optogenetics, neuromuscular system, *Caenorhabditis elegans*, guanylyl cyclases, adenylyl cyclases, rhodopsin

INTRODUCTION (775 WORDS)

Optogenetics enables the modulation of biological processes in a spatiotemporally highly defined manner within living cells and animals. To this end, photosensitive proteins are genetically targeted to specific cell types (Knopfel et al., 2010; Yizhar et al., 2011). Several optogenetic tools were developed for the manipulation of ionic currents across the plasma membrane (PM) as well as for the signalling molecules cAMP and cGMP (Gao et al., 2015; Ryu et al., 2010; Schroder-Lang et al., 2007; Tanwar et al., 2018). Both nucleotides are ubiquitous second messengers, triggering various biological responses by activating e.g. protein kinases (PKA and PKG) or cyclic nucleotide gated channels (CNGCs) (Podda & Grassi, 2014). In eukaryotic GPCR signalling, cAMP is generated predominantly by membrane-bound (mb) ACs, which are located in microdomains together with GPCRs, PK(A) and their targets (Bock et al., 2020; Cooper & Tabbasum, 2014). In rare cases, cAMP is created by soluble ACs (Buck et al., 1999). Likewise, cGMP formation is either catalysed by membrane bound, or by soluble GCs (Lucas et al., 2000).

Recently, several photoactivatable ACs and GCs (PACs and PGCs, respectively) were characterized (Gao et al., 2015; Ryu et al., 2010; Scheib et al., 2015; Stierl et al., 2011). In *C. elegans*, the microbial PACs from *Euglena* (euPAC) and *Beggiatoa* (bPAC), as well as the synthetic phytochrome-linked cyclases IlaC22 k27 and PaaC were implemented for optogenetic cAMP generation (Etzl et al., 2018; Ryu et al., 2014; Steuer Costa et al., 2017; Weissenberger et al., 2011). All are soluble proteins, thus they do not precisely mimic cAMP signalling as occurring in response to membrane bound ACs. The fungal GC rhodopsin from *Blastocladiella emersonii*, called BeCyclOp (BeRhGC, BeGC1, RhoGC) is particular in combining a rhodopsin and a GC, yielding an efficient mbGC for optogenetic cGMP generation (Avelar et al., 2015; Gao et al., 2015; Scheib et al., 2015). Another fungal CyclOp from *Catenaria anguillulae* was characterized in *Xenopus* oocytes and rat hippocampal neurons (Gao et al., 2015; Scheib et al., 2018). CyclOps facilitate research in sensory neurons, which often signal *via* cGMP (Bargmann, 2006).

Nucleotide specificity is determined by 2-3 key amino acids, and can be interconverted. Thus, highly efficient optogenetic cyclases can be turned into enzymes of the respective other nucleotide specificity. Accordingly, BeCyclOp and CaCyclOp were converted into ACs by distinct mutations (Scheib et al., 2018), as was the AC domain of bPAC, mutated into a GC and termed bPGC or BlgC (Ryu et al., 2010). The utility of nucleotidyl cyclases (NC) extends beyond their primary function as enzymes, when they are combined with CNGCs, resulting in "two-component optogenetics" (see below), as opposed to normal applications of microbial rhodopsins: These are most often used as directly light-gated ion channels or pumps to depolarize (e.g. Channelrhodopsin-2 - ChR2) or hyperpolarize (e.g. *Natronomonas pharaonis* halorhodopsin - NpHR) excitable cells (Chuong et al., 2014; Klapoetke et al., 2014), enabling investigations of basic mechanisms of synaptic transmission, or to decipher neuronal networks triggering behaviour (Han et al., 2009; Husson et al., 2012a; Oranth et al., 2018; Schultheis et al., 2011). In *C. elegans*, hyperpolarizing tools such as the proton pump archaerhodopsin-3 (Arch) from *Halorubrum sodomense*, NpHR or the *Guillardia theta* anion channel rhodopsins (GtACRs) were established (Bergs et al., 2018; Chow et al., 2010; Husson et al., 2012b; Zhang et al., 2007). However, no dedicated optogenetic tool for transport or facilitation of K^+-currents exists, with the exception of BLINK (Cosentino et al., 2015), which does not express in *C.*

elegans (our observations). To overcome some of these limitations, a two component optogenetic silencing system comprising the *Spirochaeta thermophila* cAMP-gated K^+-channel (SthK) and bPAC was implemented in several model organisms, enabling a more physiological silencing of excitable cells (Beck et al., 2018; Bernal Sierra et al., 2018).

Here, we characterize bPGC and CaCyclOp for their ability to allow optogenetic cGMP generation by co-expressing them with the TAX-2/-4 excitatory CNG channel in body wall muscle (BWM) cells of *C. elegans*. Further, we generate and characterize mbPACs with respect to their light induced cAMP production, following expression in cholinergic motor neurons and BWM cells, by assessing their influence on different behaviours of the animal. We demonstrate that mbPACs are more efficient than soluble bPAC in evoking behaviour, despite higher cAMP production of the latter, possibly because mbPACs act in close proximity to the PM. Moreover, we implement two component optogenetic systems for optical silencing, consisting of SthK or the *Blastocladiella emersonii* CNG1 (BeCNG1) K^+-channel, co-expressed with bPAC or mbPACs, respectively, and evaluate their properties and combinations for optimized utility in BWM cells and cholinergic neurons. Our work establishes a comprehensive optogenetic toolbox for cGMP and cAMP manipulations or K^+-fluxes in *C. elegans*.

METHODS

Molecular biology

The plasmids **pMS04** [pmyo-3::bPGC::SL2::mCherry], **pMS05** [pmyo-3::bPAC::SL2::mCherry], **pJN55** [pmyo-3::tax-2::GFP], **pJN58** [pmyo-3::tax-4::GFP] and **pJN63** [pmyo-3::BeCyclOp::SL2::mCherry] were described earlier (Gao et al., 2015; Woldemariam et al., 2019). The plasmid **pASH3** [pmyo-3::BeCNG1::YFP] was produced by amplification of the BeCNG1 cDNA fragment using primers BeCNG1_fwd (5`-CCGGGGATCCGCCACCATGGCTGTTGA-3`) and BeCNG1_rev (5`-GCTATAGGTACCTTCTCGAGATCCTCTTCAGGCACA-3`) and subcloning into the pmyo-3::YFP vector using *BamH*I and *Kpn*I. For **pJN67** [punc-17::BeCyclOp::SL2::mCherry], the *unc-17* promoter was amplified with primers oJN197 (5`-CCTTTTGCTCACATGGGATTACACCAATCATTTC-3`) and oJN198 (5`-TGTCCTTCATTCTAGCTGAAAATTAAATATTTTAGTG-3`) and inserted into the BeCyclOp::SL2::mCherry vector via `in-fusion cloning`. To construct **pJN68** [punc-17::BeCyclOp(A-3x)::SL2::mCherry], site-directed mutagenesis was conducted using primers oJN210 (5-`CTACAAGGTCAAAACCATCGGAGACGC-3`), oJN211 (5`-ACTCCCCAACGCTTGGCG-3`), oJN212 (5`-GACACTCGTCGGAGACACCGTC-3`) and oJN213 (5`-CAATCTGGGTTGAGGTCTCCGAG-3`). Plasmid **pJN69** [pmyo-3::BeCyclOp(A-3x)::SL2::mCherry] was generated by restriction digestion of pJN68 using *Kpn*I and *BspM*I and subcloning into the pmyo-3::BeCyclOp::SL2::mCherry backbone. To generate **pTH01** [pmyo-3::CaCyclOp(A-2x)::SL2::mCherry] and **pTH02** [pmyo-3::CaCyclOp::SL2::mCherry], the respective CaCyclOp cDNA fragments were amplified with primers oTH5 (5`-GGCGCTCTAGAATGTCTATGAAAGATAAAG-3`) and oTH6 (5`-GCGGTACCTTACTTTCTAGCGGTCAC-3`) and inserted into pmyo-3::SL2::mCherry vector using *Xba*I and *Kpn*I. **pTH04** [punc-17::CaCyclOp(A-2x)::SL2::mCherry] was produced by amplification of CaCyclOp(A-2x) fragment using primers oTH37 (5`-TCGGCTAGCCCATGTCTATGAAAGATAAAG-3`) and oTH6 (5`-GCGGTACCTTACTTTCTAGCGGTCAC-3`) and subcloning into punc-17::SL2::mCherry backbone using *Nhe*I and *Kpn*I. To construct **pTH11** [punc-17::BeCyclOp(A-2x)::SL2::mCherry], BeCyclOp fragment was amplified with primers oTH38 (5`-CAACCCACACTGGGACCTCGTCGGAGACAC-3`) and oTH39 (5`-GTGTCTCCGACGAGGTCCCAGTGTGGGTTG-3`) and inserted into punc-17::BeCyclOp[E497K]::SL2::mCherry vector using *Bcl*I and *Kpn*I. For **pTH12** [pmyo-3::BeCyclOp(A-2x)::SL2::mCherry], the BeCyclOp(A-2x) fragment was amplified using primers oTH01 (5`-GCCGTCTAGAATGAAGGACAAGGACAACAACC-3`) and oTH04 (5`-AGCCGGTACCTTACTTACGTCCGAGGACCC-3`) and subcloned into pmyo-3::SL2::mCherry backbone using *Xba*I and *Kpn*I. To generate **pTH18** [pmyo-3::SthK::mCherry], the SthK::mCherry fragment was amplified using primers oTH50 (5`-CCATCTAGAATGAAAAGCTCCGCC-3`) and oTH51 (5`-CACCTTGTAGATGAAC-3`) and inserted into the pmyo-3::mCherry vector using *Xba*I and *Sbf*I. The plasmid **pTH20** [pmyo-3::SthK::SL2::GFP] was created by amplification of the SthK fragment using primers oTH50 (5`-CCATCTAGAATGAAAAGCTCCGCC-3`) and oTH52 (5`-ATGGTACCTTATCCCCGCCGTGATG-3`) and subcloning into pmyo-3::SL2::GFP backbone using *Xba*I and *Kpn*I. To construct **pTH21** [punc-17::SthK::mCherry], the SthK::mCherry fragment was obtained by digestion with *Nhe*I and *Sbf*I and inserted into the punc17::mCherry vector. For **pTH23** [punc-17::SthK::SL2::GFP], the SthK fragment was amplified with

primers oTH53 (5`-ATGCTAGCATGAAAAGCTCCGC-3`) and oTH52 (5`-ATGGTACCTTATCCCCGCCGTGATG-3`) and subcloned into punc-17::SL2::mCherry backbone using *Nhe*I and *Kpn*I. The SL2::mCherry fragment was exchanged with SL2::GFP using *Kpn*I and *Apa*I. **pTH32** [pmyo-3::YFP::CaCyclOp(A-2x)::SL2::mCherry] was generated by amplifying YFP fragment with primers oTH69 (5`-ACGACCACTAGATCCATCTAGAATGGTGAGCAAGGGCGAGGAG-3`) and oTH71 (5`-CTTTATCTTTCATAGACATTGATCCCTTGTACAGCTCGTCCATGCC-3`) and CaCyclOp(A-2x) fragment with primers oTH72 (5`-GGACGAGCTGTACAAGGGATCAATGTCTATGAAAGATAAAG-3`) and oTH12 (5`-GACAAGCAGTTAACTAGGTG-3`), followed by insertion into the pmyo-3::SL2::mCherry vector via Gibson assembly. To construct **pTH33** [pmyo-3::YFP::BeCyclOp(A-2x)::SL2::mCherry], the YFP fragment was amplified with primers oTH69 (5`-ACGACCACTAGATCCATCTAGAATGGTGAGCAAGGGCGAGGAG-3`) and oTH70 (5`-GTTGTCCTTGTCCTTCATTGATCCCTTGTACAGCTCGTCCATG-3`) and the BeCyclOp(A-2x) fragment with primers oTH56 (5`-ATGAAGGACAAGGACAACAAC-3`) and oTH12 (5`-GACAAGCAGTTAACTAGGTG-3`). Subsequently, the fragments were inserted into the pmyo-3::SL2::mCherry backbone via Gibson assembly. **pTH41** [punc-17::YFP::BeCyclOp(A-2x)::SL2::mCherry] and **pTH42** [punc-17::YFP::BeCyclOp(A-2x)::SL2::mCherry] were generated by amplification of the YFP::CyclOp(A-2x) fragments using oTH81 (5'-CGGCTAGCATGGTGAGCAAGGG-3') and oTH12 (5'-GACAAGCAGTTAACTAGGTG-3'). Subsequently, the fragments were subcloned into punc-17::SL2::mCherry backbone using *Nhe*I and *Kpn*I.

***C. elegans* culture and transgenic animals**

Cultivation was on nematode growth medium (NGM) in the presence of the *Escherichia coli* strain OP50-1 according to standard methods (Brenner, 1974). The following strains were used or generated:

KG1180: *lite-1(ce314),* **ZX1569:** *lite-1(ce314); zxIs53[punc-17::bPAC::YFP; pmyo-2::mCherry]*, **ZX1741:** *lite-1(ce314); zxEx889[pmyo-3::tax-2::GFP, pmyo-3::tax-4::GFP, pmyo-2::mCherry],* **ZX1940:** *lite-1(ce314); zxEx960[punc-17::BeCyclOp::SL2::mCherry, pelt-2::GFP],* **ZX1941:** *lite-1(ce314); zxEx961[punc-17::BeCyclOp(A-3x)::SL2::mCherry, pelt-2::GFP],* **ZX2154:** *lite-1(ce314); zxEx1043[punc-17::CaCyclOp(A-2x)::SL2::mCherry],* **ZX2316:** *lite-1(ce314); zxEx889; zxEx1088[pmyo-3::BeCyclOp(A-3x)::SL2::mCherry],* **ZX2326:** *lite-1(ce314); zxEx1091[pmyo-3::BeCyclOp::SL2::mCherry; pmyo-3::BeCNG1::YFP],* **ZX2391:** *lite-1(ce314); zxEx1117[punc-17::BeCyclOp(A-2x)::Sl2::mCherry],* **ZX2393:** *lite-1(ce314); zxEx1119[pmyo-3::SthK::SL2::GFP; pmyo-2::mCherry],* **ZX2394:** *lite-1(ce314); zxEx1119; zxEx1120[pmyo-3::bPAC::SL2::mCherry],* **ZX2395:** *lite-1(ce314); zxEx1121 [punc-17::SthK::SL2::GFP; pmyo-3::mCherry],* **ZX2396:** *lite-1(ce314); zxEx1121; zxIs53,* **ZX2397:** *zxEx1121*, **ZX2398**: *lite-1(ce314); zxEx1122[pmyo-3::SthK::mCherry; pmyo-2::CFP],* **ZX2399:** *lite-1(ce314); zxEx1123[punc-17::SthK::mCherry; pmyo-2::CFP],* **ZX2400:** *lite-1(ce314); zxEx889; zxEx1124[pmyo-3::BeCyclOp::SL2::mCherry],* **ZX2401:** *lite-1(ce314); zxEx889; zxEx1125[pmyo-3::bPGC::SL2::mCherry],* **ZX2402:** *lite-1(ce314); zxEx889; zxEx1126[pmyo-3::CaCyclOp::SL2::mCherry],* **ZX2403:** *lite-1(ce314); zxEx889; zxEx1127[pmyo-3::BeCyclOp(A-2x)::SL2::mCherry],* **ZX2404:** *lite-1(ce314); zxEx889; zxEx1128[pmyo-3::YFP::BeCyclOp(A-2x)::SL2::mCherry],* **ZX2405:** *lite-1(ce314); zxEx889; zxEx1129[pmyo-3::CaCyclOp(A-2x)::SL2::mCherry],* **ZX2406:** *lite-1(ce314); zxEx889; zxEx1130[pmyo-3::YFP::CaCyclOp(A-2x)::SL2::mCherry],* **ZX2408:** *lite-1(ce314); zxEx889; zxEx1132[pmyo-3::bPAC::SL2::mCherry],* **ZX2504:** *lite-1(ce314); zxEx1119; zxEx1219[pmyo-3::BeCyclOp::SL2::mCherry],* **ZX2505:** *lite-1(ce314); zxEx1119; zxEx1220[pmyo-3::BeCyclOp(A-2x)::SL2::mCherry],* **ZX2506:** *lite-1(ce314); zxEx1119; zxEx1221[pmyo-3::BeCyclOp(A-3x)::SL2::mCherry],* **ZX2507:** *lite-1(ce314); zxEx1119; zxEx1222[pmyo-3::CaCyclOp(A-2x)::SL2::mCherry],* **ZX2530:** *lite-1(ce314); zxEx1119; zxEx1230[pmyo-3::BeCyclOp(A-3x)::SL2::mCherry],* **ZX2606:** *lite-1(ce314); zxEx1231[punc-17::SthK::SL2::GFP; punc-17::BeCyclOp(A-3x)::SL2::mCherry; pmyo-2::mCherry],* **ZX2607:** *lite-1(ce314); zxEx1232[punc-17::SthK::SL2::GFP; punc-17::BeCyclOp(A-3x)::SL2::mCherry; pmyo-2::mCherry],* **ZX2608:** *lite-1(ce314); zxEx1233[punc-17::SthK::SL2::GFP; punc-17::BeCyclOp(A-2x)::SL2::mCherry],* **ZX2609:** *lite-1(ce314); zxEx1124[pmyo-3::BeCyclOp::SL2::mCherry],* **ZX2610:** *lite-1(ce314); zxEx1125[pmyo-3::bPGC::SL2::mCherry],* **ZX2611:** *lite-1(ce314); zxEx1126[pmyo-3::CaCyclOp::SL2::mCherry],* **ZX2612:** *lite-1(ce314); zxEx1088[pmyo-3::BeCyclOp(A-3x)::SL2::mCherry],* **ZX2613:** *lite-1(ce314); zxEx1127[pmyo-3::BeCyclOp(A-2x)::SL2::mCherry],* **ZX2614:** *lite-1(ce314); zxEx1128[pmyo-3::YFP::BeCyclOp(A-2x)::SL2::mCherry],* **ZX2615:** *lite-1(ce314); zxEx1129[pmyo-3::BeCyclOp(A-2x)::SL2::mCherry],* **ZX2616:** *lite-1(ce314); zxEx1130[pmyo-3::YFP::BeCyclOp(A-2x)::SL2::mCherry],* **ZX2617:** *lite-1(ce314); zxEx1132[pmyo-3::bPAC::SL2::mCherry],* **ZX2659:** *lite-1(ce314); zxEx1255[punc-17::YFP::BeCyclOp(A-2x)::SL2::mCherry; pmyo-2::mCherry],* **ZX2660:** *lite-1(ce314); zxEx1256[punc-17::YFP::CaCyclOp(A-2x)::SL2::mCherry; pmyo-2::mCherry].*

Transgenic *C. elegans* were obtained by microinjection of DNA into the gonads of nematodes by standard procedures (Fire, 1986). The strain *lite-1(ce314)*, which lacks the intrinsic photophobic response, was used as background strain (Edwards et al., 2008). For ZX1741, 5.5 ng/µl of pJN55 and pJN58, and 2 ng/µl of pmyo-2::mCherry were microinjected. To create ZX2316, ZX2400-ZX2406 and ZX2609-2616, 15 ng/µl of the plasmids pJN69, pJN63, pMS04, pTH02, pTH12, pTH33, pTH01 and pTH32 were injected. ZX2408 and ZX2617 were

generated by injection of 7.5 ng/µl of pMS05. The strains ZX1940, ZX1941, ZX2154 and ZX2391 were created by injection of 30 ng/µl of pJN67, pJN68, pTH04 and pTH11. For ZX2326, 40 ng/µl of pASH3 and 15 ng/µl of pJN63 were microinjected. To generate ZX2398 and ZX2399, 10 ng/µl of pTH18 and pTH21, and 1.5 ng/µl of pmyo-2::CFP were microinjected. ZX2393 was produced by injection of 5.5 ng/µl of pTH20 and 1.5 ng/µl pmyo-2::mCherry. The strains ZX2504-ZX2507 were created by injection of 15 ng/µl of pJN63, pTH12, pJN69 and pTH01. For ZX2394, 7.5 ng/µl of pMS05 were microinjected. To create ZX2395, 5.5 ng/µl of pTH23 and 3 ng/µl pmyo-3::mCherry were injected. ZX2530 was generated by injection of 60 ng/µl of pJN69. For ZX2606, 2.5 ng/µl pTH23 and 100 ng/µl were microinjected. To obtain ZX2607 and ZX2608, 1 ng/µl pTH23 and 30 ng/µl pJN68 or 15 ng/µl pTH11 were injected. For ZX2659 and ZX2660, 30 ng/µl of pTH41 or pTH42 and 1.5 ng/µl of pmyo-2::mCherry were used.

Fluorescence microscopy

Transgenic animals were immobilized on 2% agarose pads in M9 buffer (20mM K_2PO_4; 40mM Na_2HPO_4; 80mM NaCl; 1mM $MgSO_4$) using 50 mM NaN_3 in H_2O. Expression was observed on an AxioScope.A1 (Zeiss, Germany) equipped with a 50 W (HBO) mercury lamp and *Natronomonas* halorhodopsin (NpHR) or green fluorescence protein (GFP) specific excitation/emission filter sets (AHF Analysentechnik, Germany). Images were obtained with a Hamamatsu ORCA-Flash 2.8 digital camera.

***C. elegans* behavioural assays**

Transgenic strains were kept in the dark on standard nematode growth medium (NGM) plates (5.5 cm diameter; 8 ml NGM) with OP50-1 bacteria at RT. For behavioural assays, transgenic L4 larvae were selected for fluorescence under a Leica MZ16F dissection scope and transferred to freshly seeded plates and kept in the dark. Animals supplemented with ATR were transferred to plates with OP50-1 containing 200 µM ATR. Measurements of the body length were performed as described previously (Liewald et al., 2008). Young adult animals were individually placed under red light (>600 nm) on plain NGM plates and assayed on an AxioScope.A1 microscope (Zeiss, Germany) with a 10x objective and transmission light filtered through a red 675±50nm bandpass filter. For colour illumination, the light of a 50 W HBO lamp was channelled through excitation bandpass filters of 470±40nm or 530±50nm with an intensity of 0.9 $mW*mm^{-2}$. Intensity was measured using a S120UV Sensor with PM 100D power meter (Thorlabs, Dachau, Germany). Video recordings of worms were done using a Canon G9 powershot camera. Duration of illumination was defined by a computer-controlled shutter (Sutter Instruments, USA). The body length values were calculated using a custom made workflow in KNIME (KNIME Desktop version 2.10, KNIME.com AG, 8005 Zurich, Switzerland) (Warr, 2012). Here, the length was normalized to the averaged values measured before illumination (0–5 s), and normalization was carried out for each worm. All the values below 80% or above 120% were excluded and the length-profiles were averaged for each strain. Swimming behaviour was analysed in a 96-well microtiter plate containing 100 µl of NGM and 50 µl of M9 buffer per well. Young adult animals were transferred to the microtiter plate under red light (650/50 nm) and adapted for 10 min in the dark. Video acquisition was performed with a Canon G9 powershot camera on a Axio Scope.A1 microscope (Zeiss, Germany). Animals were illuminated with an HBO 50 W lamp (Carl Zeiss AG, Germany, 470/40 nm, 530±50nm 0.2, 0.4, 1 or 1.35 $mW*mm^{-2}$) and 4x magnification. Stimulation protocol was 30 s in darkness, 30 s in light and if necessary 30 s, 60s or 270 s in darkness. Swimming cycles were counted for defined time periods of 15 s or 30 s.

Locomotion behaviour analysis on NGM plates was performed using a worm tracker as previously described (Stirman et al., 2011). A mechanical shutter (Sutter Instruments, USA) was placed between the projector and the microscope and synchronized to the light protocol. Further, the transmission light was filtered through a red 675±50nm bandpass filter and the intensity was measured using a S120UV Sensor with PM 100D power meter. Young adult animals were placed individually on NGM plates under red light (>600 nm) and kept for 15 minutes in the dark before the transfer to the worm tracker. The light protocol was 15 s dark/ 25 s light/ and 15s dark using a light intensity of 0.2 $mW*mm^{-2}$ at 470/10 nm. Speed, bending angle and body length values were calculated using a custom made workflow in KNIME as previously described (Steuer Costa et al., 2017). Speed values > 1.25 mm/s and length values which depicted deviations > 25% with respect to the mean first five seconds of the video were excluded. Videos containing > 15% of discarded data points were excluded. Speed, bending angle and body length values of each animal were normalized to the averaged values measured before illumination (0–15 s).

cNMP measurements using *C. elegans* extract

For *C. elegans* extract preparation, transgenic L4 larvae were selected for fluorescence under a Leica MZ16F dissection scope and transferred to freshly seeded OP50-1 plates containing 200 µM ATR and kept in the dark. 60 young adult animals were transferred under red light (>600 nm) into an Eppendorf tube containing 50 µl M9 buffer and 1 mM 3-Isobutyl-1-methylxanthin (IBMX, a phosphodiesterase blocker). Control animals (Dark condition) were placed for 15 min on an AxioScope.A1 microscope (Zeiss, Germany) with a 4x objective and transmission light filtered through a red 675±50nm bandpass filter. For colour illumination, the light of a 50 W HBO lamp was channelled through excitation bandpass filters of 470±40nm with an intensity of 0.5 $mW*mm^{-2}$ for 15 min.

Subsequently, the animals were subjected to three freeze-thaw cycles using liquid nitrogen. Next, the animals were vortexed with 0.25-0.5 mm glass beads for 5 min. The supernatant after centrifugation (2000 rpm, 1 min) was used for measurement of the cNMP content. cAMP was measured using AlphaScreen cAMP Detection Kit (PerkinElmer), whereas cGMP was measured using cGMP Direct Chemiluminescent ELISA Kit (Arbor Assays); for both, a CLARIOstar PLUS (BMG Labtech) Microplate Reader was used.

Data and statistical analysis

Data are depicted as mean ± SEM or mean, median, interquartile range, whiskers (1.5*IQR) and outliers, with n = number of measured animals. Statistical analyses were performed using GraphPAD Prism 8 software (GraphPad Software Inc., 7825 Fay Avenue, Suite 230 La Jolla, CA 92037;RRID:SCR_002798) or Microsoft Excel 2019 software (Microsoft Corporation, One Microsoft Way, Redmond, WA 98052-6399, USA). Student`s t-test, one-way or two-way ANOVA followed by Bonferroni correction as post hoc test were conducted, as indicated in the figure legends. P values ≤ 0.05 were determined as statistically significant.

RESULTS (2325 words)

Two component optogenetic systems for cGMP generation and depolarization comprising CyclOps or bPGC and the TAX-2/-4 CNG channel

We wanted to expand the optogenetic toolkit for cGMP generation in *C. elegans*. The previously established BeCyclOp enabled generation of a very high amount of cGMP at a high turnover rate, while the soluble bPGC produced cGMP with low efficiency and slow kinetics (Gao et al., 2015; Woldemariam et al., 2019). Thus, we were looking for a tool with features in between of BeCyclOp and bPGC. We thus generated or tested different GCs or AC mutants and compared them. To this end, we expressed the proteins in BWM cells, together with the TAX-2/-4 CNG channel, an unspecific cation channel (Komatsu et al., 1999; Ramot et al., 2008). TAX-2/-4 activation by cyclic nucleotide monophosphate (cNMP) (EC_{50}^{cGMP}= 8.4 µM; EC_{50}^{cAMP} = 300 µM, in HEK293 cells (Komatsu et al., 1999)) causes muscle depolarization and contraction, and thus a macroscopic reduction of the body length that can be measured by video microscopy (Gao et al., 2015; Liewald et al., 2008). Illumination of animals co-expressing TAX-2/-4 and CaCyclOp (from *Catenaria*) resulted in light dependent muscle contractions that by amplitude and ON-kinetics fell between of those observed in animals expressing TAX-2/-4; BeCyclOp and TAX-2/-4; bPGC (Fig. 1A, B). Thus, CaCyclOp is a useful, membrane bound alternative to bPGC, which is a soluble tool.

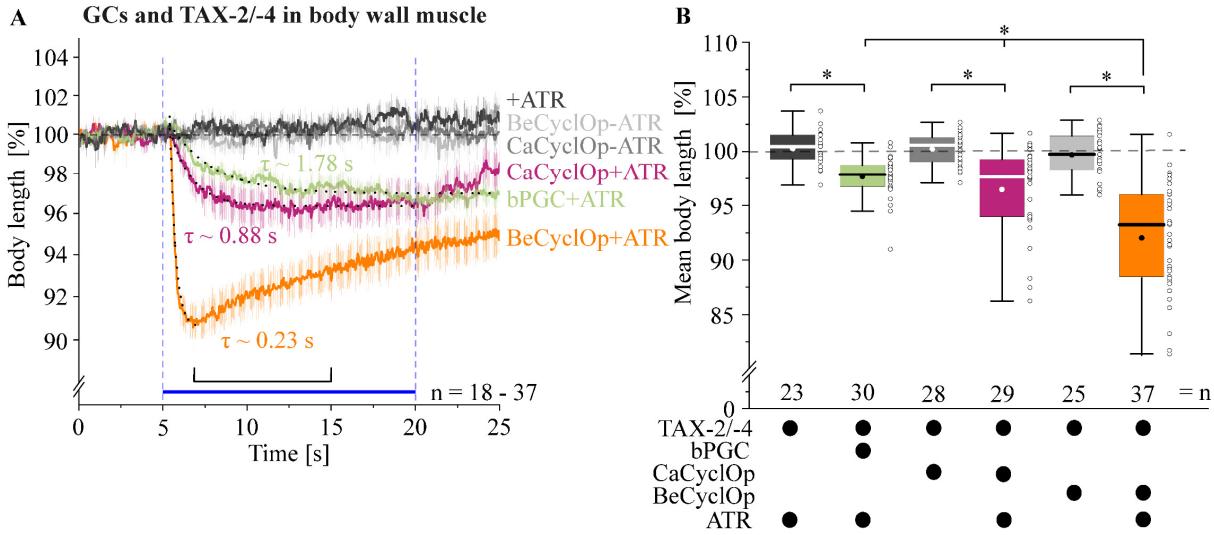

Figure 1. Characterization of light activated guanylyl cyclases with respect to CNG-channel mediated muscle contraction. (A) Body length measurements (normalized to the initial length ±SEM) of animals co-expressing the TAX-2/-4 CNG channel and either BeCyclOp, CaCyclOp or bPGC in body wall muscle cells before, during and after a 15 s light pulse (0.9 $mW*mm^{-2}$; 470 nm). Animals were supplemented with (+) or without (-) ATR (all-*trans* retinal). Onset-time constants were determined by fitting as mono-exponential decay (dotted lines). (B) Group analysis for the data in A during light stimulation (6.5-15 sec). Displayed are the interquartile range (IQR), median (—), mean values (●), individual measurements (○) and whiskers (1.5*IQR). n = number of animals. Blue bar indicates period of illumination. Statistically significant differences determined by one-way ANOVA/Bonferroni correction: $^{*}p<0.05$.

Implementation and analysis of membrane-bound PACs in cholinergic motor neurons

For the generation of mbPACs, the GC domains of BeCyclOp and CaCyclOp were mutated by distinct changes into AC domains (Linder, 2005; Ryu et al., 2010; Sunahara et al., 1998): BeCyclOp(E497K/C566D), termed "BeCyclOp(A-2x)"; BeCyclOp(E497K/H564D/C566T) = "BeCyclOp(A-3x)" and CaCyclOp(E497K/C566D) = "CaCyclOp(A-2x)". Previously we showed that cAMP generation in cholinergic motor neurons via bPAC caused increased neurotransmission and has profound effects on locomotion behaviour (Steuer Costa et al., 2017). Thus, we used this bPAC induced behaviour as a positive control, and to compare the effectiveness of the engineered mbPACs. The induced behavioural change could be assessed by the swimming frequency in liquid, and by determination of crawling speed and body bending on solid media (Steuer Costa et al., 2017; Weissenberger et al., 2011). Illumination of animals expressing BeCyclOp(A-2x) or bPAC in cholinergic neurons evoked comparably increased swimming cycles and crawling speeds (BeCyclOp(A-2x) appeared even more efficient), however, the effects induced by bPAC decayed faster than for BeCyclOp(A-2x) (Figures 2B, C, E, F, S1A, E, F). In contrast to bPAC, light stimulation of BeCyclOp(A-2x) expressing animals depicted no change in their mean bending angles and only a small decrease in body length (Figures 2I, J, S3E, G, H, J). For CaCyclOp(A-2x) and BeCyclOp(A-3x) expressing animals, no light evoked change in their swimming behaviour was observed (Figures 2B, C, S1B, D, F). With the exception of CaCyclOp(A-2x) expressing animals, all analysed PACs effected decreased basal swimming frequency as compared to the genetic background *lite-1(ce314)* (*lite-1* was used since these animals lack intrinsic photophobicity; Figure S1E, F). Whether this is due to basal (dark) activity of the cyclases, or a potential burden due to expression of the foreign protein is unclear, but see below for cAMP measurements in extracts (Figure 3F). Further, BeCyclOp(A-2x) expressing animals depicted decreased basal crawling speed, independent of the addition of ATR (Figure S3B, D).

To possibly improve expression and/or membrane targeting of the mbPACs, BeCyclOp(A-2x) and CaCyclOp(A-2x) were fused N-terminally with yellow fluorescent protein (YFP; Scheib et al., 2018). For YFP::CaCyclOp(A-2x), this improved effects strongly, turning it into a tool as useful as BeCyclOp(A-2x). In both cases, expression of the protein reduced the basal swimming frequency compared to the genetic background (*lite-1(ce314)*), (Figures 2D, G, H, K, L, S4, S5). Our analyses show differences in the triggered behavioural output between the soluble bPAC and the engineered mbPACs (crawling speed, swimming cycles, body contraction evoked by stimulation of BWMs): BeCyclOp(A-2x); YFP::BeCyclOp(A-2x) and also YFP::CaCyclOp(A-2x) are as efficient or even more powerful as the soluble bPAC, while details in the parameters of their action may enable choosing one tool over another for specific applications (Figure 8, Table S1, Table S2).

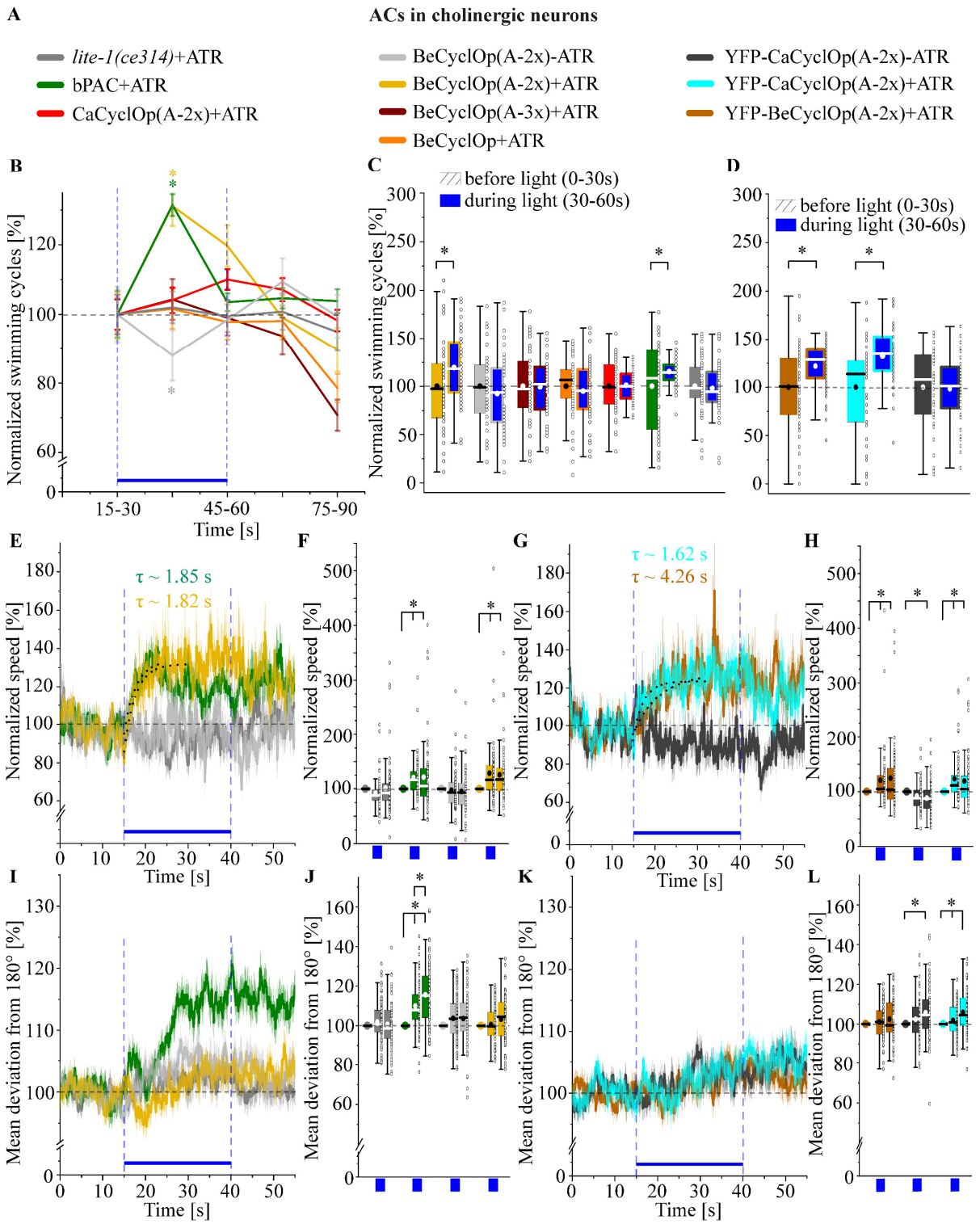

Figure 2. Characterizing membrane bound photoactivatable adenylyl cyclases in cholinergic motor neurons via induced effects on locomotion. (A) Colour code for the analysed strains in B-L. (B) Normalized swimming cycles (±SEM) of animals expressing bPAC, BeCyclOp(A-2x), BeCyclOp(A-3x), wild type BeCyclOp, or CaCyclOp(A-2x) in cholinergic motor neurons of *C. elegans*, in the genetic background *lite-1(ce314)*, during and after a 30s light pulse (0.2 mW*mm^{-2}; 470 nm). The swimming cycles are normalized to the mean swimming frequency 15s before light application (n = 40-50). (C, D) Mean swimming cycles 30s before and 30s during illumination of the animals in B (C, n = 40-50), and of animals expressing YFP::BeCyclOp(A-2x) or YFP::CaCyclOp(A-2x) (D, n = 39-52), normalized to the mean swimming frequency 30s before the light stimulus. (E, G) Time course of the speed (normalized to the first 15 s without light; ±SEM) of the genetic background *lite-1(ce314)* and animals expressing bPAC or BeCyclOp(A-2x) (E), or YFP::BeCyclOp(A-2x) or YFP::CaCyclOp(A-

2x) (G) (E: n = 47-72; G: n = 47-64). (F, H) Mean normalized speed of the time periods before (0-15s), during (15-40s; blue bar) and after (40-55s) illumination (0.2 $mW*mm^{-2}$; 470 nm). (F: n = 66-72; H: n = 58-61). (I, K) Normalized bending angles (±SEM) of the animals in E, G (I: n = 47-72; K: n = 47-64). (J, L) Mean normalized bending angles before, during, and after light. (J: n = 66-72; L: n = 58-61). n = number of animals. The blue bars indicate the period of illumination. Shown in C, D, F, H, J, L are the interquartile range (IQR), median (—), mean values (●), individual measurements (○) and whiskers (1.5*IQR). Statistically significant differences determined by one-way ANOVA and Student`s t test (B, C, D) or one-way ANOVA/Bonferroni correction (E-L): $^{*}p<0.05$.

Evaluating cGMP vs. cAMP production by membrane bound PACs

The behavioural analysis of animals expressing mbPACs provided a strong indication that these tools indeed generated cAMP. However, the actual extent of the specificity change, and the potential of remaining cGMP production could not be analysed accurately this way. Thus, to further evaluate the mbPACs for their yield of optogenetic cNMP production, they were co-expressed with the TAX-2/-4 CNG channel in BWM cells of *C. elegans*. This channel is mostly specific for cGMP; it can also be activated by cAMP, though with 200-fold lower sensitivity. We thus used body length measurements to assess the possibly remaining cGMP production, as well as induced cAMP production in animals expressing TAX-2/-4 and the respective mbPAC (Gao et al., 2015). With exception of CaCyclOp(A-2x), that was ineffective, light stimulation (2 s, 535 nm) of all mbPACs evoked similar overall body contraction (Figure 3B, C). Importantly, none of the mbPACs induced contractions as effectively as BeCyclOp, in line with the largely reduced activation of the CNG channel by cAMP. Slight differences in the light triggered behavioural changes induced by the mbPACs are present in the time course, while the effect induced by TAX-2/-4; BeCyclOp(A-2x) expressing animals decayed much more slowly (Figure 3B). Interestingly, in contrast to CaCyclOp(A-2x), YFP::CaCyclOp(A-2x) could mediate a light triggered body contraction, whereas in comparison to BeCyclOp(A-2x), YFP::BeCyclOp(A-2x) exhibited a faster decay of the evoked effect (Figure 3B). To further classify the cNMP production generated by BeCyclOp(A-2x), we compared changes in the body lengths due to light application (2s, 470 nm) between TAX-2/-4; BeCyclOp(A-2x) and TAX-2/-4; bPAC expressing animals. Here, bPAC induced a stronger body contraction, indicating higher overall cAMP production than the mbPAC (Figure 3D, E). We note that some BeCyclOp(A-2x) expressing animals had altered morphology, i.e. shortened body length and an increased mid body width, for unknown reasons. Such animals were excluded from our analyses.

Because both cGMP and cAMP can activate the TAX-2/-4 CNG channel, leaving some ambiguity in the interpretation of the above results, we wanted to use a more defined assay probing for cAMP and cGMP production and specificity. We thus employed in *vitro* assays for cAMP and cGMP quantification. Here, for BeCyclOp(A-2x), YFP::BeCyclOp(A-2x) and YFP::CaCyclOp(A-2x), we could determine a high level of cAMP produced in transgenic *C. elegans* tissue, though not reaching the same extent as the soluble bPAC (bPAC produced ca. 2.5 x more cAMP than YFP::BeCyclOp(A-2x); dark activity could not be determined with this assay, as cAMP levels in dark were as in non-transgenic controls). Importantly, none of the mbPACs showed any measurable cGMP production (Figure 3F, G; S6). For GCs, cGMP production was highest for BeCyclOp, while bPGC and CaCyclOp were comparable, generating ca. 4.5 times less cGMP than BecyclOp. In sum, the novel engineered optogenetic

cAMP tools produce cAMP at high levels in *vivo*, with high specificity, while BeCyclOp is the best cGMP producing optogenetic tool.

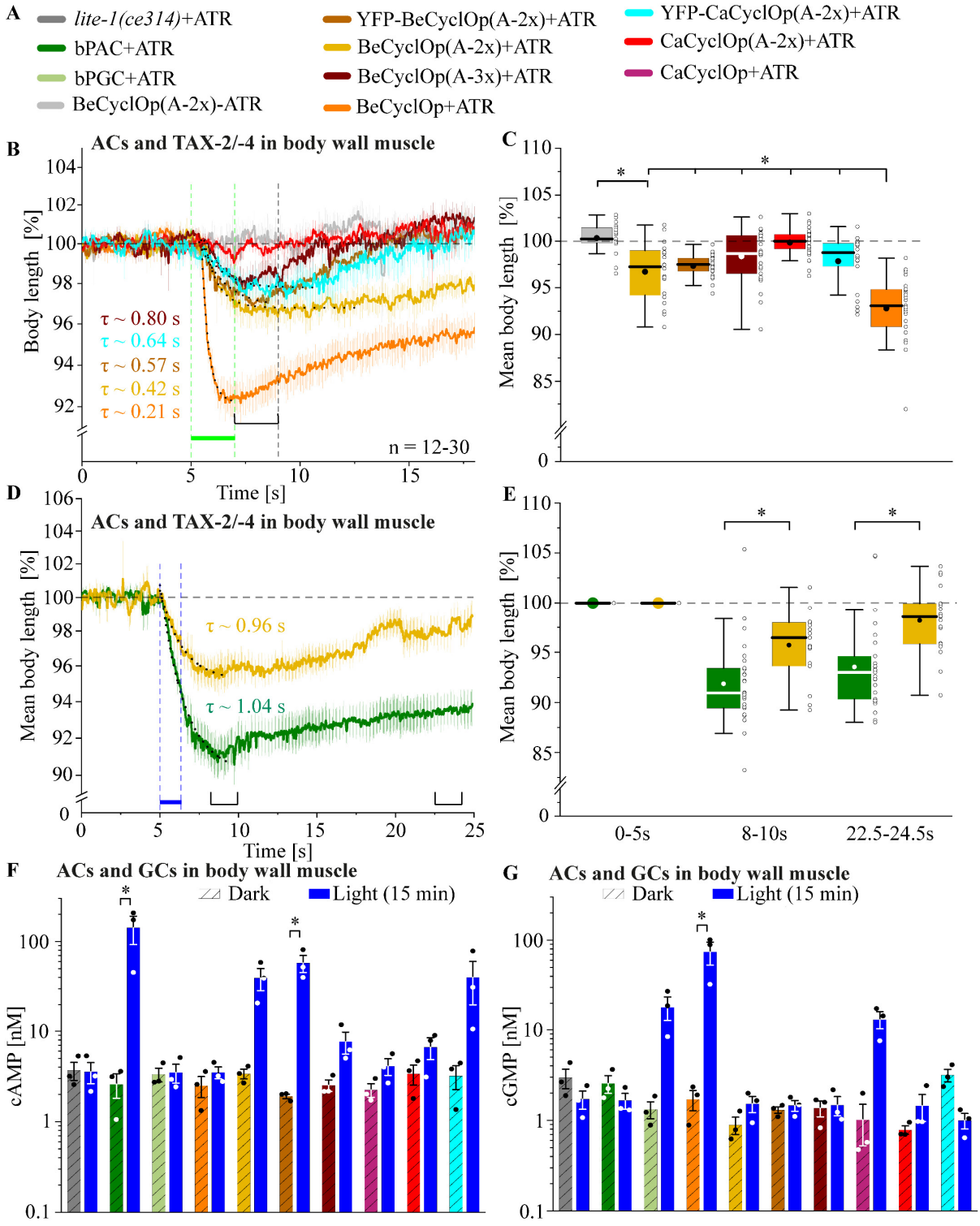

Figure 3. mbPACs and the TAX-2/-4 CNG channel in body wall muscle cells show different efficiency and kinetics in cNMP generation.(A) Colour code for the investigated strains in B-G (all strains express the TAX-2/-4 CNG channel). (B) Body lengths (±SEM) of TAX-2/-4-expressing animals, co-expressing BeCyclOp(A-2x), YFP::BeCyclOp(A-2x), BeCyclOp(A-3x), wild type BeCyclOp, CaCyclOp(A-2x) or YFP::CaCyclOp(A-2x) in body wall muscle cells, before and after a 2 s light pulse (0.9 mW*mm^{-2}; 535 nm). Time constants were calculated by non-linear fitting for mono-exponential decay of the body lengths (dotted lines). (C) Body length reductions

after light application (7-9s), triggered by optogenetic cNMP generation and TAX-2/-4 activation (n = 17-27). (D) Body length measurements (±SEM) of animals, co-expressing TAX-2/-4 and either BeCyclOp(A-2x) or bPAC before and after a 2 s light pulse (0.9 $mW*mm^{-2}$; 470 nm) (n = 16-27). (E) Mean normalized body lengths for the time periods before (0-5s), during (8-10s) and after (22.5-24.5s) light stimulation (n = 19-28). (F, G) Quantification of cAMP (F) and cGMP (G) levels using *C. elegans* extracts. Animals, expressing bPAC, bPGC, BeCyclOp, BeCyclOp(A-2x), YFP::BeCyclOp, BeCyclOp(A-3x), CaCyclOp, CaCyclOp(A-2x) or YFP::CaCyclOp(A-2x) were illuminated with blue light (5 $mW*mm^{-2}$; 470 nm, 15 min), or incubated with red filtered transmission light (675nm; 15 min) as dark condition. Displayed are the mean values (±SEM) including the individual measured values (●). n = 3 samples of 60 animals each. In C, E the interquartile range (IQR), median (─), mean values (●), individual measurements (○) and whiskers (1.5*IQR) are shown. The green and blue bar indicate the period of illumination Statistically significant differences determined by one-way ANOVA/Bonferroni correction (B-E) or two-way ANOVA/Bonferroni correction: $^{*}p<0.05$.

Combining BeCyclOp and the cGMP-gated K^+-channel BeCNG1 for K^+-based cell hyperpolarization.

Recently, the cGMP-gated K^+-channel BeCNG1 was found in the genome of the aquatic fungus *Blastocladiella emersonii*, and characterized as the effector protein downstream of BeCyclOp, participating in the phototactic response of the zoospore (Avelar et al., 2015). We wanted to adopt this mechanism to achieve optogenetic hyperpolarization using K^+-conductance, for which only few examples have been demonstrated so far. We thus co-expressed BeCyclOp and the BeCNG1 channel in BWM cells (Figure 4A, B) to obtain a two-component optogenetic system for the manipulation of K^+-currents. Optogenetic cGMP production should activate the BeCNG1 channel, thus triggering muscle hyperpolarization and body elongation (Gao et al., 2015; Liewald et al., 2008). BeCNG1::YFP showed a clustered appearance along the muscle membrane (Figure 4A). Illumination of animals co-expressing BeCNG1 and BeCyclOp, supplemented with ATR, evoked a slightly increased body length within ~3 s, which remained at this level even after turning light off (Figure 4C, D). No effects were observed in control animals cultivated without ATR. As we showed earlier, animals expressing only BeCyclOp do not exhibit changes in body length (Gao at al., 2015). In conclusion BeCyclOp and BeCNG1 achieved moderate, but long-lasting optogenetic hyperpolarization of BWM cells of *C. elegans*.

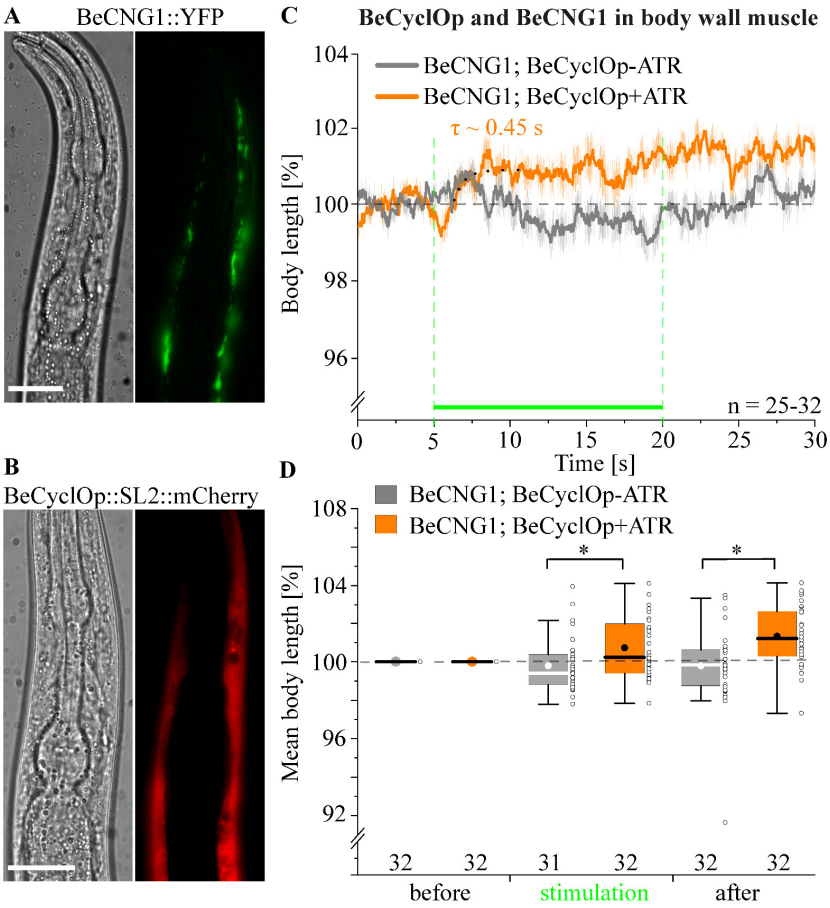

Figure 4. BeCyclOp and the cGMP-gated BeCNG1 K⁺-channel trigger muscle hyperpolarization. Co-expression of BeCNG1::YFP (A) and BeCyclOp::SL2::mCherry (B) in BWMs of *C. elegans*. Scale bar, 50 µm. (C) Body length measurements (±SEM) of animals, co-expressing BeCNG1 and BeCyclOp, supplemented with (+) or without (-) ATR before, during and after a 15 s light pulse (0.9 mW*mm^{-2}; 535 nm). Onset-time constant was determined by fitting as mono-exponential growth (dotted line). (D) Group data, mean normalized body lengths for the time periods before (0-5s), during (5-20s) and after (20-30s) light application. Displayed are the interquartile range (IQR), median (—), mean values (●), individual measurements (○) and whiskers (1.5*IQR). n = number of animals. The green bar indicates the period of illumination. Statistically significant differences determined by one-way ANOVA/Bonferroni correction: $^{*}p<0.05$.

Implementation of the cAMP-gated K⁺-channel SthK and bPAC in BWM cells.

Previously, a two component optogenetic silencing system, consisting of bPAC and the cAMP-gated SthK channel from *Spirochaeta thermophila*, was used to manipulate K⁺-currents in various model organisms (Beck et al., 2018; Bernal Sierra et al., 2018). To analyse the functionality of this system in *C. elegans*, we co-expressed the SthK channel and bPAC in BWM cells (Figure 5A) and performed behavioural experiments, i.e. swimming and body length measurements. Muscle hyperpolarization decreases swimming frequency, and increases body length (Zhang et al., 2007). Expressing the SthK channel alone reduced the basal swimming frequency as compared to the genetic background *lite-1(ce314)*, likely due to intrinsic cAMP, and this was further decreased by co-expression with bPAC, even in the dark, arguing for effects of the known dark activity of bPAC (Figure 5B). Illumination of SthK; bPAC expressing animals, however, caused a complete arrest of their swimming behaviour (Figure 5B). In body length measurements, light stimulation caused long lasting elongation of ca. 4%, i.e. comparable to other strong hyperpolarizers like GtACR2 or Arch (Bergs et al., 2018;

Husson et al., 2012b), within ~1 s (Figure 5C, D), which lasted up to 10 min (Figure S7), possibly, as *C. elegans* BWM expresses no or only low levels of phosphodiesterases. In conclusion, bPAC and SthK evoked light dependent, robust, long-term muscle hyperpolarization. However, SthK is so sensitive that intrinsic cAMP levels already suffice for its activation.

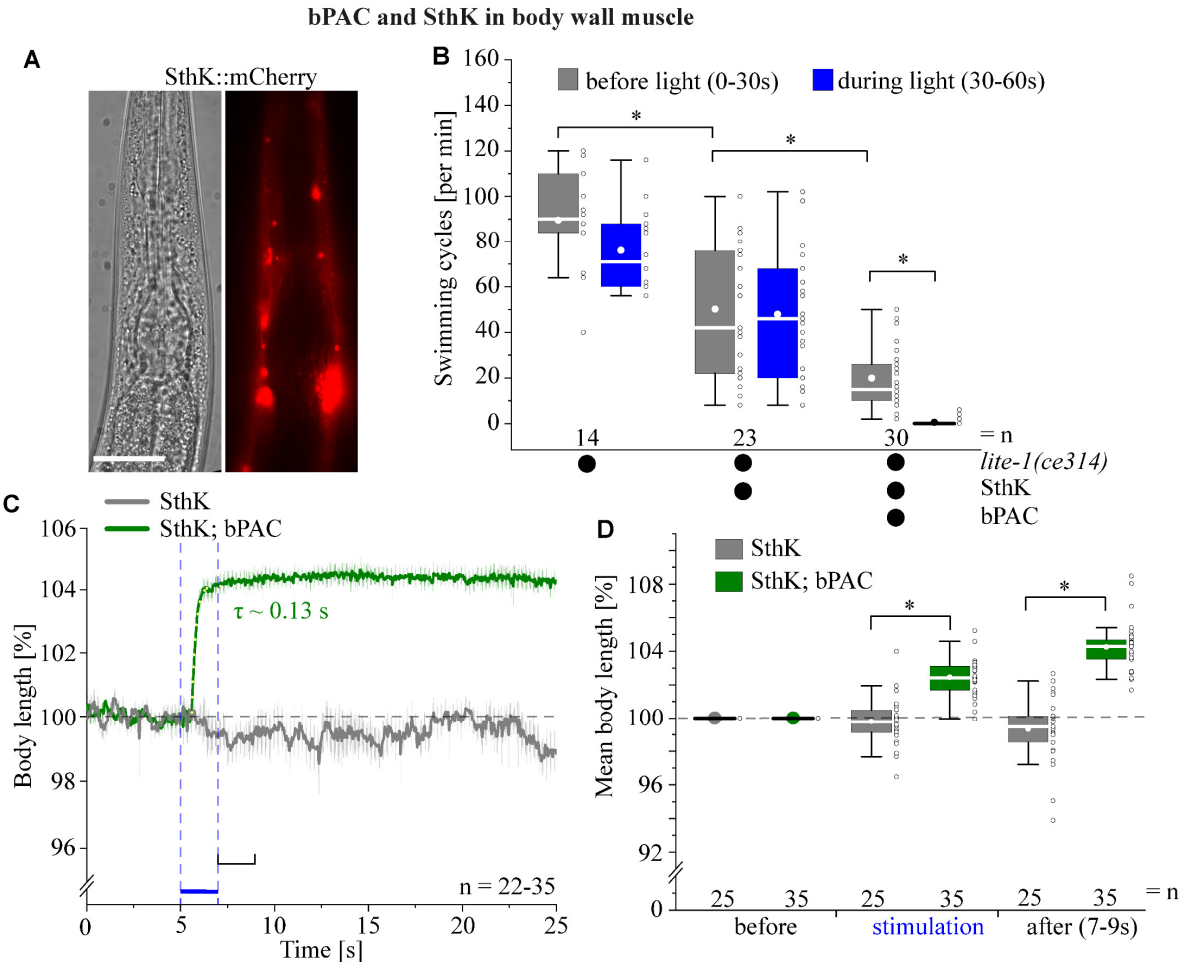

Figure 5. Establishment of the SthK channel and bPAC as a two component optogenetic system for the manipulation of K^+-currents in BWM cells. (A) Fluorescence micrograph (right) and DIC brightfield image (left) of the head of an animal expressing SthK::mCherry in BWM cells (anterior is up). Scale bar, 50 µm. (B) Swimming behaviour of animals expressing either SthK alone, or co-expressing SthK and bPAC, as well as the genetic background *lite-1(ce314)*. Swimming cycles (±SEM) were calculated 30 s before, and 30 s during light stimulation (0.2 $mW*mm^{-2}$; 470 nm). Displayed are the interquartile range (IQR), median (—), mean values (●), individual n values (○) and whiskers (1.5*IQR). (C) Body length measurements (±SEM) of animals, expressing either SthK alone, or co-expressing SthK and bPAC before and after a 2 s light pulse (0.9 $mW*mm^{-2}$; 470 nm). Onset-time constant was determined by fitting as mono-exponential growth (dotted line). (D) Mean normalized body lengths before (0-5s), during (5-7s) and after (7-9s) illumination. Shown are the interquartile range (IQR), median (—), mean values (●), individual measurements (○) and whiskers (1.5*IQR). n = number of animals. The blue bar indicates the period of illumination. Statistically significant differences determined by one-way ANOVA and Student`s t test (B) and one-way ANOVA/Bonferroni correction (D): $^*p<0.05$.

mbPACs enable more precise control of the SthK channel for inhibition in BWM cells

Because the SthK channel is very sensitive and activated by very low levels of cAMP, and bPAC produces very high amounts of cAMP and exhibits dark activity, we combined SthK with the engineered variants of the cyclase rhodopsins. These should have no dark activity and produce lower amounts of cAMP, as shown in our in vitro assays (Figures 3F, G, S6A, B). We

co-expressed the SthK channel with the CyclOp PACs (mbPACs) in BWM cells and investigated their hyperpolarizing potential and light control using swimming assays and body length measurements. First, we investigated the parental cyclase, BeCyclOp, in combination with SthK. Interestingly, illumination of animals co-expressing SthK and wild type BeCyclOp increased the swimming cycles and decreased the body length, possibly because cGMP acts an antagonist (Kesters et al., 2015), or agonist with low efficacy (Schmidpeter et al., 2018), or due to a transient depletion of ATP (due to cGMP generation) and thus disinhibition of the cells due to reduced basal cAMP levels and thus reduced SthK activation (Figure 6A-C).
Next, we tested the mbPAC variants, as these produce lower amounts of cAMP and could thus lead to preferable outcome in the evoked effects on muscle hyperpolarization. Animals co-expressing SthK and BeCyclOp(A-2x) showed a high variability in their swimming frequency, independent of the addition of ATR, which was not observed for SthK; BeCyclOp(A-3x) animals (Figure 6A). In contrast to this, SthK; CaCyclOp(A-2x) expressing animals depicted a decreased basal swimming frequency in comparison to SthK expressing animals (Figure 6A). Illumination of the SthK; BeCyclOp(A-2x) and (A-3x) variant expressing animals reduced the swimming cycles, however, it did not trigger a complete arrest (Figure 6A). Also, light stimulation of these animals increased the body length (Figure 6B, C). Whereas for SthK; BeCyclOp(A-3x) animals the evoked hyperpolarization reached a higher level and decayed a few seconds after turning off light, it remained constant for SthK; BeCyclOp(A-2x) animals (Figure 6B). For SthK; CaCyclOp(A-2x) animals, light application slightly decreased the swimming rate, and had no influence on their body length (Figure 6A-C). Overall, the combination SthK and BeCyclOp(A-3x) appears to be the most favourable for K^+-based inhibition: It had no influence on the basal swimming rate, and light triggered a strong inhibition and body elongation. As light did not trigger a complete arrest of swimming, we tried to improve this by increasing the expression level of BeCyclOp(A-3x). However, this reduced the basal swimming cycles independent of ATR supplementation (Figure S8), thus expression levels need to be titrated for optimal performance.

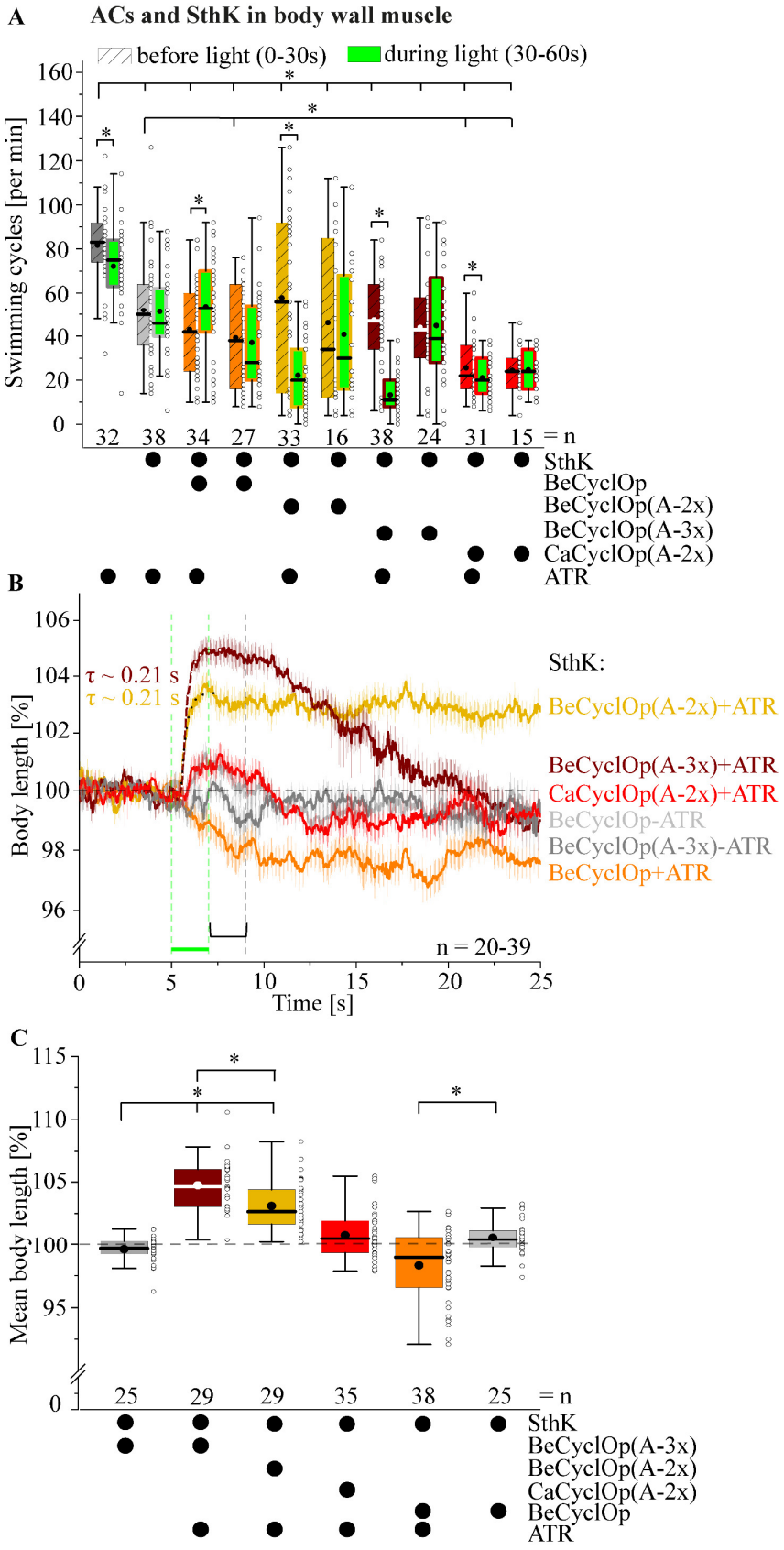

Figure 6. Membrane bound PACs and SthK as tools for the manipulation of K⁺-currents. (A) Swimming behaviour of animals expressing the SthK channel alone, or with wild type BeCyclOp, BeCyclOp(A-2x), BeCyclOp(A-3x) or CaCyclOp(A-2x), respectively, in the genetic background *lite-1(ce314)*. Swimming cycles (±SEM) were calculated 30 s before and 30 s during light application (1 mW*mm^{-2}; 535 nm). (B) Body lengths (±SEM) of animals, co-expressing SthK and wild type BeCyclOp, BeCyclOp(A-2x), BeCyclOp(A-3x) or

CaCyclOp(A-2x) before and after a 2 s light pulse (0.9 mW*mm^{-2}; 535 nm). Onset-time constants were determined by fitting as mono-exponential growth (dotted line). (C) Mean normalized body lengths of the animals shown in (B) after light stimulation (7-9s). Shown in A and C are the interquartile range (IQR), median (—), mean values (●), individual n values (○) and whiskers (1.5*IQR). n = number of animals. The green bar indicates the period of illumination. Statistically significant differences determined by one-way ANOVA and Student`s t test (A) and one-way ANOVA/Bonferroni correction (C): *p<0.05.

PACs and the SthK channel in cholinergic neurons

Last, we assessed the SthK and PAC systems for their ability to hyperpolarize *C. elegans* cholinergic neurons, by analysing swimming behaviour. Like in muscle, expression of the SthK channel decreased the basal swimming rate in the genetic background *lite-1(ce314)* and in wild type animals (as expected due to cAMP intrinsic signalling in these neurons; Steuer Costa et al., 2017), which was further reduced by co-expression with bPAC and the likely increased cAMP levels due to its dark activity (Figure 7B). Illumination of these animals declined the swimming frequency to nearly complete arrest (Figure 7B, C). This effect was long lasting, and the swimming rate increased again after 90-150s following the end of the illumination (Figure 7C). Since the reduction of swimming rate by SthK and bPAC co-expression was substantial already in the dark, this combination of tools appears of limited use in *C. elegans*, unless one wants to achieve permanent K^+-based inhibition. Thus, we investigated if co-expression of SthK with BeCyclOp(A-2x) or BeCyclOp(A-3x) would be an alternative for this cell type. Using the same expression level of SthK as used before, no viable mbPAC transgenes were obtained. Consequently, we reduced the expression level of SthK. Still, all transgenes effected decreased of basal swimming rates (Figure 7D), though not as much as for SthK expressed at higher levels. Light stimulation of these animals evoked a further, robust decrease in swimming frequency, which increased again after turning off light (Figure 7D, E). Best results were obtained with BeCyclOp(A-2x) with lowest SthK expression. In sum, SthK in combination with bPAC or the BeCyclOp PACs are able to hyperpolarize cholinergic neurons in *C. elegans*, however, they also affect the physiology, likely the resting potential of the neurons.

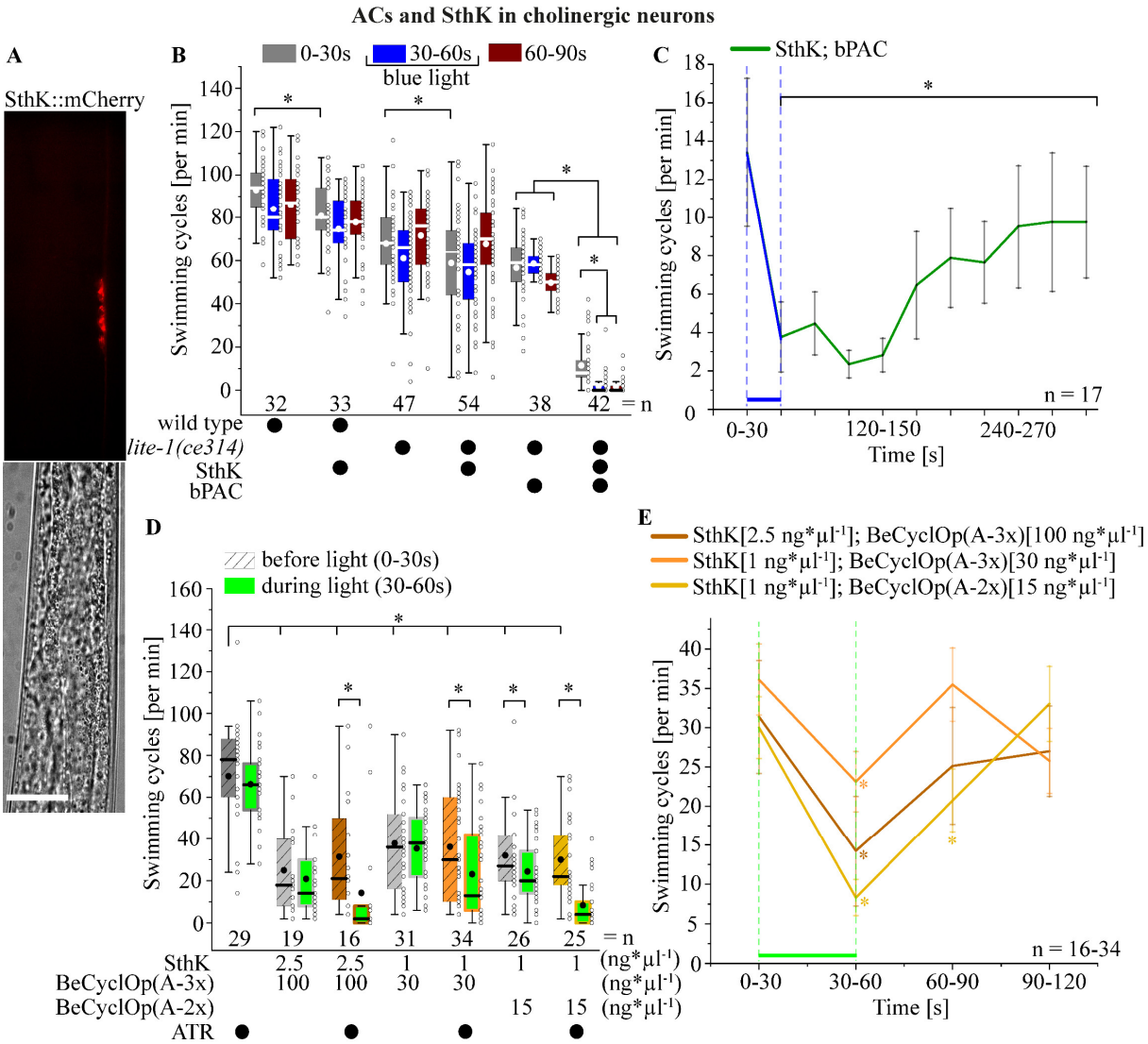

Figure 7. Application of bPAC or mbPACs and the SthK channel for hyperpolarization of cholinergic neurons. (A) Expression of SthK::mCherry in cholinergic neurons of *C. elegans*. Scale bar is 50 µm. (B) Swimming behaviour (±SEM) analysis of animals, expressing SthK, bPAC, or co-expressing SthK and bPAC, the genetic background *lite-1(ce314)* and wild type animals, 30s before and 30s after a 30s light pulse (0.4 mW*mm^{-2}; 470 nm). (C) Swimming cycles (±SEM) of animals, co-expressing SthK and bPAC 30s before and 270s after 30s light application (0.4 mW*mm^{-2}; 470 nm). (D) Swimming frequency (±SEM) of animals, co-expressing the SthK channel and BeCyclOp(A-3x) or BeCyclOp(A-2x) in the genetic background *lite-1(ce314)*, 30s before and during a 30s light pulse (1.35 mW*mm^{-2}; 535 nm). Strains were generated using different amounts of plasmid DNA (indicated by ng*µl^{-1}). (E) Swimming behaviour (±SEM) analysis of animals in D, 30s before and 60s after a 30 s light pulse (1.35 mW*mm^{-2}; 535 nm). In B, D, the interquartile range (IQR), median (—), mean values (●), individual measurements (○) and whiskers (1.5*IQR) are shown. n = number of animals. The green and blue bars indicate the period of illumination. Statistically significant differences determined by one-way ANOVA and Student`s t test (B, D, E) and paired Student`s t test (C): *p<0.05.

DISCUSSION (1179 words)

In this study, we present a comprehensive optogenetic toolbox for cGMP and cAMP manipulation in excitable cells of *C. elegans*, as well as a combination with depolarizing and K^+-specific hyperpolarizing CNG channels for two-component optogenetics. We analysed the *C. anguillulae* CyclOp for its efficiency in optogenetic cGMP production, and characterised engineered adenylyl cyclases, emerging by conversion of the guanylyl cyclase domains of

BeCyclOp and CaCyclOp, for light induced cAMP generation in *C. elegans*. These tools were combined with different cNMP-gated channels and assessed for their potential to activate or silence body wall muscle cells or cholinergic neurons, highlighting different combinations with different levels of activity, kinetics and long- or short-lasting effects, such that researchers can choose the appropriate tool for their specific application (Figure 8).

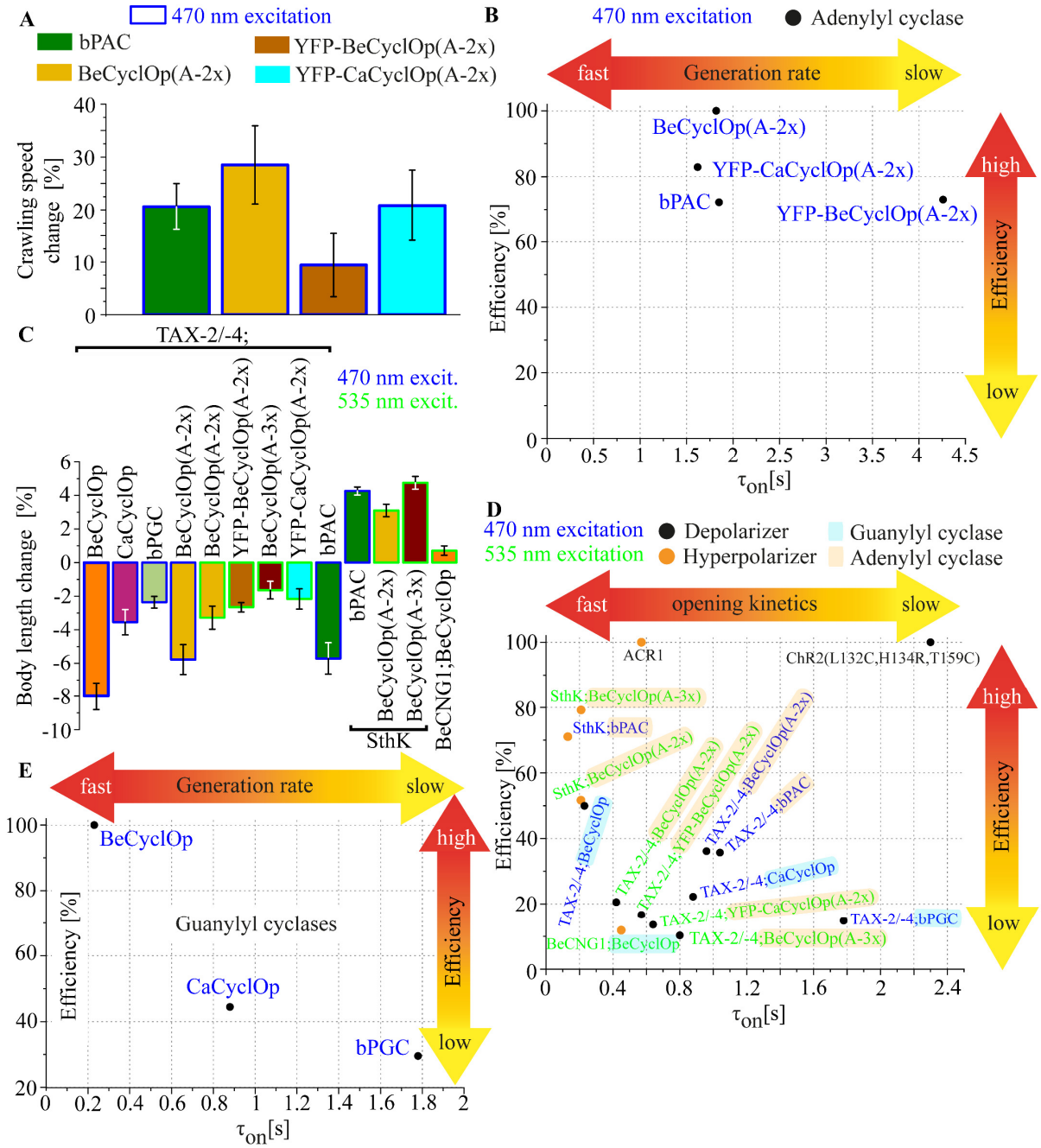

Figure 8. Evaluation of guanylyl and adenylyl cyclases, as well as de- and hyperpolarizing two-component optogenetic tools characterized in this paper. (A) Changes in crawling speed triggered by adenylyl cyclases. Depicted is the mean normalized speed (±SEM) relative to the initial crawling speed of the animal. (B) Scheme of photoactivatable adenylyl cyclases expressed in cholinergic neurons, classified by the time course of evoked behavioural changes, as a proxy for cAMP generation rate (τ) and efficiency. The efficiency was calculated as follows: Comparison of crawling speed changes, induced by the respective tool (0.2 mW*mm^{-2}; 470 nm), relative to the maximum crawling speed increase. The best performing tool (BeCyclOp(A-2x)) was arbitrarily set to100 % efficiency. (C) Body length changes evoked by de- and hyperpolarizing combinations of cyclases and CNG

channels, as indicated. Shown is the mean normalized body length (±SEM) relative to the initial body length of the animal. (D) Scheme of optogenetic de- and hyperpolarizer two-component optogenetic tools, as well as ChR2 and ACR1 'benchmarks', expressed in body wall muscle cells, categorized by opening kinetics (τ) and efficiency. The efficiency was estimated as follows: Depolarizer (hyperpolarizer) - comparison of body length reduction (increase), evoked by the respective tool (0.9 $mW*mm^{-2}$; 470 nm; 535 nm) relative to the maximum body length decrease (elongation). 100 % efficiency was arbitrarily set for the best performing optogenetic tools in such assays, ChR2(L132C, H134R, T159C) and ACR1 (Bergs et al., 2018). E) Photoactivatable guanylyl cyclases expressed with the TAX-2/-4 CNG channel in body wall muscle, classified by the time course of evoked behavioural changes, as a proxy for cGMP generation rate (τ) and efficiency. The efficiency was calculated as follows: Comparison of body length changes, induced by the respective tool (0.9 $mW*mm^{-2}$; 470 nm), relative to the initial body length. The best performing tool (BeCyclOp; see panel C) was arbitrarily set as being 100 % efficient.

Until now, BeCyclOp was the only mbPGC implemented in *C. elegans* (Gao et al., 2015). cGMP generation by BeCyclOp is characterized by a high magnitude reached within a few seconds (Gao et al., 2015; Scheib et al., 2015). Depending on the cell type in which the tool is expressed, application could be accompanied by over-activation of cGMP signalling pathways or by cross-talk to cAMP signalling or NTP utilizing pathways, e.g. due to macroscopic depletion of GTP or NTPs via interconverting enzymes, thus interfering with the cellular output or metabolism of the cell. To overcome this problem, we characterized CaCyclOp, which is less efficient than BeCyclOp (Gao et al., 2015), for its applicability in *C. elegans*: CaCyclOp showed lower light inducible cGMP production, slower cGMP production rate, but similarly high substrate specificity, when compared to BeCyclOp. Thus, CaCyclOp enables fine-tuning of cGMP levels, which makes it a beneficial optogenetic tool for future studies of cGMP signalling, comprising mbPGCs for signal transmission. Specific subcellular targeting would allow studies of cGMP signalling closer to physiological conditions, allowing its application in *C. elegans* research areas such as sensory signalling and plasticity, or regulation of the dauer arrest (Bargmann & Horvitz, 1991; Birnby et al., 2000; Fielenbach & Antebi, 2008; Schultheis et al., 2011). Our test system, in combination with the possibility to study subcellular cGMP signalling within a living organism, would further support the development of mbPGCs and their application in higher organisms with a need for spatial and temporal control of cGMP levels, not only through subcellular localization of PDEs (Bock et al., 2020; Houslay, 2010), but also by local photoactivation, thus allowing new insights into cellular processes such as cell growth and survival.

Previously, the existing optogenetic tools for cAMP generation in *C. elegans* were soluble proteins. These did not mimic the physiological conditions under which cAMP is produced by mbACs within microdomains in close vicinity to the PM (Bock et al., 2020; Cooper, 2003; Etzl et al., 2018; Ryu et al., 2014; Steuer Costa et al., 2017; Weissenberger et al., 2011). To generate mbPACs, we used CyclOps and converted them into ACs by specific mutations. Amongst the analysed mbPACs, the YFP::CyclOps and BeCyclOp(A-2x) depicted the highest magnitudes of light triggered cAMP production, though not reaching the extent produced by bPAC, and no obvious residual cGMP generation. Interestingly, besides the desired enhanced locomotion behaviour, we observed differences between behavioural changes induced by local (YFP::CyclOps; BeCyclOp(A-2x)) and cytosolic (bPAC) cAMP signalling in cholinergic neurons, i.e. increased diversity of the behavioural output (bending angles, body length; for speed, mbPACs were slightly more effective than bPAC) and a more rapidly decaying response (swimming and crawling behaviour) for cytosolic cAMP signalling. The latter could be a hint

that PDEs do not access cAMP generated in the vicinity of the membrane as readily as cAMP in the cytosol. Generally, undesired cAMP signalling pathways may be activated by cytosolic cAMP generation, thus triggering changes in the bending angles and body length. In contrast, local (membrane proximal) optogenetic cAMP production may more specifically activate cAMP dependent neurotransmission, i.e. increased mobilization and priming/docking of synaptic vesicles (SV) and an increased filling of the SVs with ACh (due to neuropeptide signalling; Steuer Costa et al., 2017) and thus an increase in locomotion behaviour.
In contrast to CaCyclOp(A-2x), expression of wild type BeCyclOp, mbPAC variants and bPAC reduced the basal swimming frequency, which could be due to a common 'toxicity' of these proteins, or due to cNMP production in the dark. Furthermore, expression of BeCyclOp(A-2x) in cholinergic neurons reduced the basal crawling speed, and in some cases expression in muscle cells changed the morphology of the animals. These observations are independent of ATR addition, thus indicating (some) constitutive cAMP production by this variant, which was also reported before (Trieu et al., 2017). However, as expression of bPAC in cholinergic neurons reduced the basal swimming frequency too, and the YFP::CyclOp variants showed the highest tolerability in these neurons, they constitute the preferred optogenetic tools, and may facilitate studies e.g. in neuropeptidergic signalling, memory formation or cell growth. Activation of BeCyclOp(A-3x) in cholinergic neurons evoked no obvious behavioural changes, however, a light dependent increase in cAMP by expression in muscle cells (co-expressed with TAX-2/-4 or SthK) could be detected. Due to the generation of low amounts of cAMP, this variant could be of interest for future studies of cAMP signalling (Rost et al., 2017).
Generation of second messengers is accompanied by amplification of the primary signal, making combinations of photoactivated nucleotide cyclases (PNCs) and CNG channels useful tools due to a reduced need for light. Aiming on multi component systems for the depolarization of excitable cells, we combined the TAX-2/-4 CNG channel with PNCs. In this context, none of the analysed systems were able to induce comparably high depolarization effects as the previously implemented TAX-2/4; BeCyclOp system in regard of the magnitude (Gao et al., 2015), however, in contrast to this system, no desensitization was observed for TAX-2/-4 combined with BeCyclOp(A-2x), CaCyclOp or bPGC. Yet, these systems require the expression of three genes, making them less versatile than ChR2. Because no optogenetic silencing tool on the basis of transport or facilitation of K^+-currents in *C. elegans* exists, we characterized two component optogenetic systems composed from a cNMP-gated channel and a PNC for their potential to hyperpolarize BWM cells and/or cholinergic neurons. Here, the system composed of the cGMP-gated BeCNG1 channel and BeCyclOp was able to slightly hyperpolarize BWM cells. Its potential to hyperpolarize other cell types still has to be investigated. In case of the system comprising the cAMP-gated SthK channel, expression of the channel alone reduced the basal swimming frequency of the animals, independent of the cell type (muscle or cholinergic motor neurons), indicating a pre-activation of the channel due to intrinsic cAMP. Also, co-expression with the PACs further reduced the basal swimming frequency (with the exception of BeCyclOp(A-3x) in BWMs), emphasizing the high affinity of SthK for cAMP, and a low dark activity of the PACs. Though the SthK-PAC system achieved strong and long-lasting hyperpolarizing effects, its applicability is restricted to cell types not containing intrinsic cAMP. To overcome this problem, SthK variants with specific mutations

in the cAMP binding pocket might be helpful, to generate a channel with decreased cAMP affinity, that may then be used to obtain a more controllable tool for optogenetic silencing.

Acknowledgements

We thank Suely Gomes for providing the BeCNG1 plasmid. We acknowledge critical comments by members of the Gottschalk lab. We are indebted to H. Fettermann, F. Baumbach, R. Wagner for expert technical assistance, and F. Becker, W. Steuer Costa, A. Hammer and N. Ho for technical help and help with data analysis.

References

Avelar GM, Glaser T, Leonard G, Richards TA, Ulrich H, & Gomes SL (2015). A Cyclic GMP-Dependent K+ Channel in the Blastocladiomycete Fungus Blastocladiella emersonii. Eukaryotic cell 14**:** 958–963.

Bargmann CI (2006). Chemosensation in C. elegans. WormBook.

Bargmann CI, & Horvitz HR (1991). Control of larval development by chemosensory neurons in Caenorhabditis elegans. Science 251**:** 1243-1246.

Beck S, Yu-Strzelczyk J, Pauls D, Constantin OM, Gee CE, Ehmann N*, et al.* (2018). Synthetic Light-Activated Ion Channels for Optogenetic Activation and Inhibition. Frontiers in neuroscience 12**:** 643.

Bergs A, Schultheis C, Fischer E, Tsunoda SP, Erbguth K, Husson SJ*, et al.* (2018). Rhodopsin optogenetic toolbox v2.0 for light-sensitive excitation and inhibition in Caenorhabditis elegans. PLoS One 13**:** e0191802.

Bernal Sierra YA, Rost BR, Pofahl M, Fernandes AM, Kopton RA, Moser S*, et al.* (2018). Potassium channel-based optogenetic silencing. Nature communications 9**:** 4611.

Birnby DA, Link EM, Vowels JJ, Tian H, Colacurcio PL, & Thomas JH (2000). A Transmembrane Guanylyl Cyclase (DAF-11) and Hsp90 (DAF-21) Regulate a Common Set of Chemosensory Behaviors in Caenorhabditis elegans. Genetics 155**:** 85-104.

Bock A, Annibale P, Konrad C, Hannawacker A, Anton SE, Maiellaro I*, et al.* (2020). Optical Mapping of cAMP Signaling at the Nanometer Scale. Cell 182**:** 1519-1530 e1517.

Brenner S (1974). The genetics of Caenorhabditis elegans. Genetics 77**:** 71-94.

Buck J, Sinclair ML, Schapal L, Cann MJ, & Levin LR (1999). Cytosolic adenylyl cyclase defines a unique signaling molecule in mammals. PNAS 96**:** 79–84.

Chow BY, Han X, Dobry AS, Qian X, Chuong AS, Li M*, et al.* (2010). High-performance genetically targetable optical neural silencing by light-driven proton pumps. Nature 463**:** 98-102.

Chuong AS, Miri ML, Busskamp V, Matthews GAC, Acker LC, Sørensen AT*, et al.* (2014). Noninvasive optical inhibition with a red-shifted microbial rhodopsin. Nature neuroscience 17**:** 1123–1129.

Cooper DM, & Tabbasum VG (2014). Adenylate cyclase-centred microdomains. Biochem J 462**:** 199-213.

Cooper DMF (2003). Regulation and organization of adenylyl cyclases and cAMP. The Biochemical Journal 375**:** 517–529.

Cosentino C, Alberio L, Gazzarrini S, Aquila M, Romano E, Cermenati S*, et al.* (2015). Optogenetics. Engineering of a light-gated potassium channel. Science 348**:** 707-710.

Edwards SL, Charlie NK, Milfort MC, Brown BS, Gravlin CN, Knecht JE*, et al.* (2008). A novel molecular solution for ultraviolet light detection in Caenorhabditis elegans. PLoS Biol 6**:** 0060198.

Etzl S, Lindner R, Nelson MD, & Winkler A (2018). Structure-guided design and functional characterization of an artificial red light-regulated guanylate/adenylate cyclase for optogenetic applications. The Journal of biological chemistry 293**:** 9078–9089.

Fielenbach N, & Antebi A (2008). C. elegans dauer formation and the molecular basis of plasticity. Genes Dev 22**:** 2149-2165.

Fire A (1986). Integrative transformation of Caenorhabditis elegans. Embo J 5**:** 2673-2680.

Gao S, Nagpal J, Schneider MW, Kozjak-Pavlovic V, Nagel G, & Gottschalk A (2015). Optogenetic manipulation of cGMP in cells and animals by the tightly light-regulated guanylyl-cyclase opsin CyclOp. Nature communications 6.

Han X, Qian X, Bernstein JG, Zhou H-H, Franzesi GT, Stern P*, et al.* (2009). Millisecond-timescale optical control of neural dynamics in the nonhuman primate brain. Neuron 62**:** 191–198.

Houslay MD (2010). Underpinning compartmentalised cAMP signalling through targeted cAMP breakdown. Trends in Biochemical Sciences 35**:** 91-100.

Husson SJ, Costa WS, Wabnig S, Stirman JN, Watson JD, Spencer WC*, et al.* (2012a). Optogenetic Analysis of a Nociceptor Neuron and Network Reveals Ion Channels Acting Downstream of Primary Sensors. Curr Biol 22**:** 743-752.

Husson SJ, Liewald JF, Schultheis C, Stirman JN, Lu H, & Gottschalk A (2012b). Microbial Light-Activatable Proton Pumps as Neuronal Inhibitors to Functionally Dissect Neuronal Networks in C. elegans. PLoS ONE 7**:** e40937.

Kesters D, Brams M, Nys M, Wijckmans E, Spurny R, Voets T*, et al.* (2015). Structure of the SthK carboxy-terminal region reveals a gating mechanism for cyclic nucleotide-modulated ion channels. PLoS One 10**:** e0116369.

Klapoetke NC, Murata Y, Kim SS, Pulver SR, Birdsey-Benson A, Cho YK*, et al.* (2014). Independent optical excitation of distinct neural populations. Nature methods 11**:** 338–346.

Knopfel T, Lin MZ, Levskaya A, Tian L, Lin JY, & Boyden ES (2010). Toward the second generation of optogenetic tools. J Neurosci 30**:** 14998-15004.

Komatsu H, Jin Y-H, L'Etoile N, Mori I, Bargmann CI, Akaike N*, et al.* (1999). Functional reconstitution of a heteromeric cyclic nucleotide-gated channel of Caenorhabditis elegans in cultured cells. Brain Research 821**:** 160–168.

Liewald JF, Brauner M, Stephens GJ, Bouhours M, Schultheis C, Zhen M*, et al.* (2008). Optogenetic analysis of synaptic function. Nat Methods 5**:** 895-902.

Linder JU (2005). Substrate selection by class III adenylyl cyclases and guanylyl cyclases. IUBMB life 57**:** 797–803.

Lucas KA, Pitari GM, Kazerounian S, Ruiz-Stewart I, Park J, Schulz S*, et al.* (2000). Guanylyl Cyclases and Signaling by Cyclic GMP. Pharmacological Reviews 52**:** 375–413.

Oranth A, Schultheis C, Tolstenkov O, Erbguth K, Nagpal J, Hain D*, et al.* (2018). Food Sensation Modulates Locomotion by Dopamine and Neuropeptide Signaling in a Distributed Neuronal Network. Neuron 100**:** 1414-1428 e1410.

Podda MV, & Grassi C (2014). New perspectives in cyclic nucleotide-mediated functions in the CNS: the emerging role of cyclic nucleotide-gated (CNG) channels. Pflugers Arch 466**:** 1241-1257.

Rost BR, Schneider-Warme F, Schmitz D, & Hegemann P (2017). Optogenetic Tools for Subcellular Applications in Neuroscience. Neuron 96**:** 572-603.

Ryu M-H, Kang I-H, Nelson MD, Jensen TM, Lyuksyutova AI, Siltberg-Liberles J*, et al.* (2014). Engineering adenylate cyclases regulated by near-infrared window light. Proceedings of the National Academy of Sciences of the United States of America 111**:** 10167–10172.

Ryu M-H, Moskvin OV, Siltberg-Liberles J, & Gomelsky M (2010). Natural and engineered photoactivated nucleotidyl cyclases for optogenetic applications. The Journal of biological chemistry 285**:** 41501–41508.

Scheib U, Broser M, Constantin OM, Yang S, Gao S, Mukherjee S*, et al.* (2018). Rhodopsin-cyclases for photocontrol of cGMP/cAMP and 2.3 A structure of the adenylyl cyclase domain. Nature communications 9**:** 2046.

Scheib U, Stehfest K, Gee CE, Korschen HG, Fudim R, Oertner TG*, et al.* (2015). The rhodopsin-guanylyl cyclase of the aquatic fungus Blastocladiella emersonii enables fast optical control of cGMP signaling. Science signaling 8**:** rs8.

Schmidpeter PAM, Gao X, Uphadyay V, Rheinberger J, & Nimigean CM (2018). Ligand binding and activation properties of the purified bacterial cyclic nucleotide-gated channel SthK. J Gen Physiol 150**:** 821-834.

Schroder-Lang S, Schwarzel M, Seifert R, Strunker T, Kateriya S, Looser J*, et al.* (2007). Fast manipulation of cellular cAMP level by light in vivo. Nat Methods 4**:** 39-42.

Schultheis C, Liewald JF, Bamberg E, Nagel G, & Gottschalk A (2011). Optogenetic long-term manipulation of behavior and animal development. PLoS One 6**:** e18766.

Steuer Costa W, Yu S-C, Liewald JF, & Gottschalk A (2017). Fast cAMP Modulation of Neurotransmission via Neuropeptide Signals and Vesicle Loading. Current biology : CB 27**:** 495–507.

Stierl M, Stumpf P, Udwari D, Gueta R, Hagedorn R, Losi A*, et al.* (2011). Light modulation of cellular cAMP by a small bacterial photoactivated adenylyl cyclase, bPAC, of the soil bacterium Beggiatoa. J Biol Chem 286**:** 1181-1188.

Stirman JN, Crane MM, Husson SJ, Wabnig S, Schultheis C, Gottschalk A*, et al.* (2011). Real-time multimodal optical control of neurons and muscles in freely behaving Caenorhabditis elegans. Nat Methods 8**:** 153-158.

Sunahara RK, Beuve A, Tesmer JJG, Sprang SR, Garbers DL, & Gilman AG (1998). Exchange of Substrate and Inhibitor Specificities between Adenylyl and Guanylyl Cyclases. The Journal of biological chemistry 273**:** 16332–16338.

Tanwar M, Sharma K, Moar P, & Kateriya S (2018). Biochemical Characterization of the Engineered Soluble Photoactivated Guanylate Cyclases from Microbes Expands Optogenetic Tools. Applied biochemistry and biotechnology 185**:** 1014–1028.

Trieu MM, Devine EL, Lamarche LB, Ammerman AE, Greco JA, Birge RR*, et al.* (2017). Expression, purification, and spectral tuning of RhoGC, a retinylidene/guanylyl cyclase fusion protein and optogenetics tool from the aquatic fungus Blastocladiella emersonii. J Biol Chem 292**:** 10379-10389.

Warr WA (2012). Scientific workflow systems: Pipeline Pilot and KNIME. J Comput Aided Mol Des 26**:** 801-804.

Weissenberger S, Schultheis C, Liewald JF, Erbguth K, Nagel G, & Gottschalk A (2011). PACα--an optogenetic tool for in vivo manipulation of cellular cAMP levels, neurotransmitter release, and behavior in Caenorhabditis elegans. Journal of neurochemistry 116**:** 616–625.

Woldemariam S, Nagpal J, Hill T, Li J, Schneider MW, Shankar R*, et al.* (2019). Using a Robust and Sensitive GFP-Based cGMP Sensor for Real-Time Imaging in Intact Caenorhabditis elegans. Genetics 213**:** 59-77.

Yizhar O, Fenno LE, Davidson TJ, Mogri M, & Deisseroth K (2011). Optogenetics in neural systems. Neuron 71**:** 9-34.

Zhang F, Wang L-P, Brauner M, Liewald JF, Kay K, Watzke N*, et al.* (2007). Multimodal fast optical interrogation of neural circuitry. Nature 446**:** 633–639.